

# Beyond Jack-Ups: A Moonshot for Future Offshore Wind Turbine Installation Vessels for an Uncertain Market

J.J. de Ridder<sup>1,2,\*</sup>, J.D. Stroo<sup>2</sup>, and A.A. Kana<sup>3</sup>

## ABSTRACT

*This paper addresses the growing offshore wind market's demand for larger turbines in deeper waters by highlighting limitations in existing installation solutions and proposing a new concept with a floating monohull, named Moonshot, which will thus be different than traditional jack-up or semi-submersible crane installation vessel options. This paper discusses the design process, which combines Ulstein Rotterdam's Controlled Innovation and Blended Design to develop the concept. This process is used to explore various market scenarios to determine optimal vessel parameters. Results demonstrate how optimizing for financial performance or seakeeping behavior impacts the design. Moonshot's initial parameters are established, and its performance is compared to existing installation solutions.*

## KEY WORDS

Early-stage design; Complex design methods, Design space exploration; Offshore wind turbine installation; Seakeeping.

## INTRODUCTION

Today's society faces growing concern over climate change, which is primarily caused by the release of greenhouse gases and other hazardous emissions. Generating electricity and heat by burning fossil fuels causes a large part of global emissions (United Nations n.d.). To help mitigate the impacts of climate change, it is crucial to reduce the reliance on fossil fuels and transition to cleaner, renewable energy sources. One of those sources is offshore wind energy. As a result, offshore wind energy is a rapidly growing industry. The global wind market has experienced significant growth in recent years, with the total installed capacity increasing from zero in the 1990s to over 40 GW in 2020. This growth is expected to continue towards 630 GW in 2050 (Kuhn, et al 2023).

Due to the improvement in offshore wind energy and growing demand, the landscape of the offshore wind turbines is also changing. Analysis of 4C Offshore wind farm data (February 24, 2023) has been performed, revealing three major trends. The first is the increasing capacity of turbines. The turbine capacity has significantly increased over the last years and is expected to continue to increase. With the increasing capacity of turbines, the physical size of turbines also increases, making them larger and heavier. The second is the increasing distance from shore to the offshore wind farms (OWFs). The main reason for this is that available location near the coast, especially in the North Sea, are getting scarce (WindEurope 2020). Also, wind speeds are higher and thus more favorable (Nikitas, et al 2020). From 2011 to 2023, the average distance from land to OWF has more than doubled (NORWEP 2022). The third is the increase in water depths at OWF locations. The analysis showed that water depth was not more than 20 meters in 2010, while nowadays the water depth is almost 40 meters. The wind farm data showed that this number is expected to increase in the future.

Currently, wind turbine and foundation transportation and installation (T&I) is done by the same vessels. However, due to the increasing weight and size of foundations, which are growing faster than turbines, foundation installation work is shifting to purpose-built foundation installation vessels (FIVs) (Foxwell 2022). Wind turbine installation will therefore soon be done by dedicated wind turbine installation vessels (WTIVs). This research is thus focused on the process of wind turbine installation. Other research focused on understanding the driving factors behind offshore wind installation vessels includes van Lynden et al (2020). There are various ways of T&I for offshore wind turbines. Seven distinctive methods were identified for offshore wind turbine installation with vessels, as shown in Figure 1.

---

<sup>1</sup> Department of Maritime and Transport Technology, Delft University of Technology, Delft, The Netherlands

<sup>2</sup> Ulstein Design and Solutions B.V., Rotterdam, The Netherlands

<sup>3</sup> Department of Maritime and Transport Technology, Delft University of Technology, Delft, the Netherlands; ORCID: 0000-0002-9600-8669

\* Corresponding Author: jesse.deridder@ulstein.com

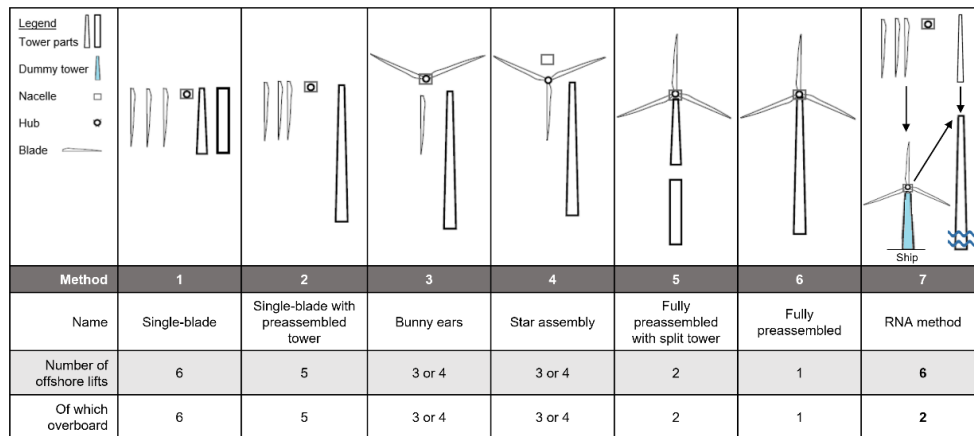


**Figure 1: Overview of common methods for offshore wind turbine installation, based on (Jiang 2021, Richmond et al 2018, EnergyFacts.eu 2019)**

The methods mainly differ on the number of onshore preassembled components and subsequently the number of required lifts. The method and degree of preassembly influences the number of offshore lifts. Since offshore lifts are risky and susceptible to delay or damage due to wind conditions, the preference is to minimize offshore assembly (Kaiser, et al 2011; Iberdrola n.d.). Also, from a cost perspective it is beneficial to reduce the number of lifts offshore. For example, (Robinson, et al 2022) state that if construction costs would be \$1 onshore, it is \$2 in port, and \$10 offshore. Despite, most offshore wind turbines are currently installed using method 2 – single blade with preassembled tower - (Asgarpour, 2016) because components can be transported more easily and deck space is used most-efficiently, reducing the number of required roundtrips (Kaiser, et al 2011). Method 7 is a novel installation method which combines the advantages of method 2 and method 6, ensuring efficient use of deck space, while also keeping the number of overboard offshore lifts as low as possible. The rotor nacelle assembly (RNA) is assembled on board of the vessel in a controlled environment with a dummy tower.

Regarding transportation of turbine components, there are two options. The first option is all-in-one, in which the installation vessel both transports and installs the turbine components. The vessel loads at the marshalling port and sails to the installation site. There, the components are installed by the same vessel. When empty, the vessel returns to the marshalling port, repeating the cycle (Vis, et al 2016). The second option is a feeder system, in which the WTIV stays at the OWF location and is supplied by feeder barges or vessels that shuttle between the marshalling port and OWF to be loaded and unloaded with turbine components. An advantage of this strategy is that installation vessel's productivity could be higher because it does not have to sail. However, lifting from another vessel at sea, which is moving due to waves, could be very risky (Vis, et al 2016), potentially damaging the fragile turbine components (Asgarpour 2016).

Currently, mostly jack-up vessels are used for wind turbine T&I (Asgarpour 2016). These vessels can elevate themselves above the sea surface with their legs to provide a stable (Nørkaer Sørensen, 1984) base for lifting operations and eliminate vessel and crane displacements due to waves and surges (Streatfeild, et al 2013; Attari, et al 2014). Analysis of the existing fleet of jack-up vessels used for wind turbine T&I with the 4C Offshore wind vessel database (March 10, 2023), showed that they will not be able to lift the next-generation turbines. Furthermore, the increasing water depths are a negative progression for jack-ups. The leg length of these vessel dictates the maximum working depth (Attari, et al 2014). In addition, because of their interaction with the seabed, they are dependent on soil conditions. A seabed survey must be done beforehand, requiring other vessels (Riviera Newsletters 2010), and these vessels cannot be deployed at all locations. In addition, lowering and raising the legs takes up a considerable amount of time (Uraz 2011), especially considering that this must be done at every turbine location and in port. This makes jack-ups very inefficient.

Alternatively, floating solutions are also sometimes used for wind turbine installation, such as semi-submersible crane vessels (SSCVs). A major drawback of these vessels is that their day rates are very high (Jiang 2021) and their capabilities exceed what is needed for offshore wind turbine installation (Kaiser, et al 2011), making them cost-inefficient. In addition, these vessels require a feeder system, despite having a substantial deck area. This is because SSCVs have a transit draft of 10 to 12 meters. Their maximum draft, during lifting operations, ranges from 25 to 32 meters (Saipem n.d.; Heerema Marine Contractors 2020), while the water depth at marshalling ports is typically not larger than 9 to 13 meters (Parkinson, et al 2022). As a result, SSCVs are not able to enter the marshalling ports to load turbine components, requiring a feeder system with all risks associated.

Multiple ways to address the gap between the existing wind turbine installation fleet and the market demands were investigated. Vessels currently on order or being built were found to be just larger jack-ups. Existing jack-ups are being retrofitted with larger cranes to be able to install the next-generation turbines. However, these approaches do not address the installation bottlenecks associated with jacking. In addition, several new concepts for future wind turbine installation were researched. These concepts were found to be mostly floating installation solution, relying on fully preassembled

installation methods, reducing the number of offshore overboard lifts. However, there are stability and seakeeping risks when sailing with a fully preassembled turbine (Herman 2002; Díaz, et al 2023). Most of the concepts were found to still have installation bottlenecks, such as the jacking or the need for a feeder system. Also, most concepts were found to have complex hull types, such as semi-submersibles or catamarans, which are expensive to build, leading to higher day rates (Djupevåg Eri 2015). Additionally, operational costs are generally higher for these hull types (Schouten 2018).

Based on the market, concept analysis, and previous development with industry partners, it was concluded that there is a need for a new cost-effective and efficient solution. This research proposes a new floating monohull vessel concept, called Moonshot, to address the gap between future market demand and current and near-term solutions. Monohulls generally have a large open deck area and are therefore capable of carrying a lot of cargo. Also, day rates are lower than for the other types of WTIVs (Jiang 2021). Also, they are capable of higher transit speeds than, for example, jack-ups and SSCVs (Djupevåg Eri 2015). But most of all, this vessel type would not have any of the mentioned installation bottlenecks. However, a floating monohull would be more susceptible to motions because of waves during the installation of the turbines, which is important to consider.

The aim of this research is to explore the feasibility of Moonshot and to investigate how it can be developed into a viable concept. Because of the unpredictable nature of the market it will operate in, it is important to explore the design space of Moonshot and elucidate optimal design parameters for both financial performance and seakeeping performance. The main research question of this paper is: “What should optimal design parameters be for the innovative Moonshot concept, a floating monohull vessel for offshore wind turbine installation, taking into account financial and seakeeping performance, while considering the uncertainties and evolving requirements of the offshore wind market?”

## DEVELOPING MOONSHOT

To design Moonshot, it is important to choose a suitable design strategy. Multiple design strategies were investigated. These included: point-based design, set-based design, systems engineering, systems-based design, and optimization-based design. Each of these design strategies were evaluated on several aspects that are important for the development of Moonshot, including: (1) applicability in ship design, (2) the degree of innovation the strategy enables, (3) optimization with a parametric ship model, and (4) flexibility in dealing with changing requirement and market uncertainty. None of the design strategies was found to meet all requirements. In response to this, two strategies developed by Ulstein Design & Solutions B.V. (UDSBV) were introduced: Controlled Innovation (CI) and Blended Design. When investigating these strategies, it was found that they are amalgamations of the main state-of-the-art design strategies.

CI was originally developed by Van Bruinessen (2016) as part of his PhD dissertation and is a strategy to evaluate functions and design aspects in the ship design process. The application of development packages for high-risk design aspects allows for knowledge generation and often results in new solutions and an improved design. Therefore, this method proves to be very useful when innovating in the realm of ship design. Blended Design was developed by Zwaginga (2020), Zwaginga et al (2021) and allows for multi-parameter optimization for many variations of a parent ship design within different (market) scenarios, while considering the lifetime financial performance.

The two strategies have been combined into one design strategy, suitable for the development of Moonshot. CI is used to determine the functions of Moonshot, as well as to establish the underlying design aspects. These design aspects are then evaluated to identify which ones require additional focus or extra knowledge. It is then important to differentiate between the design aspects that should be addressed in the development packages of the CI process and those that can be handled through Blended Design. The results obtained from the development packages will eventually serve as input or boundaries for Blended Design. The adopted design strategy for this research is shown in Figure 2 and described in more detail below.

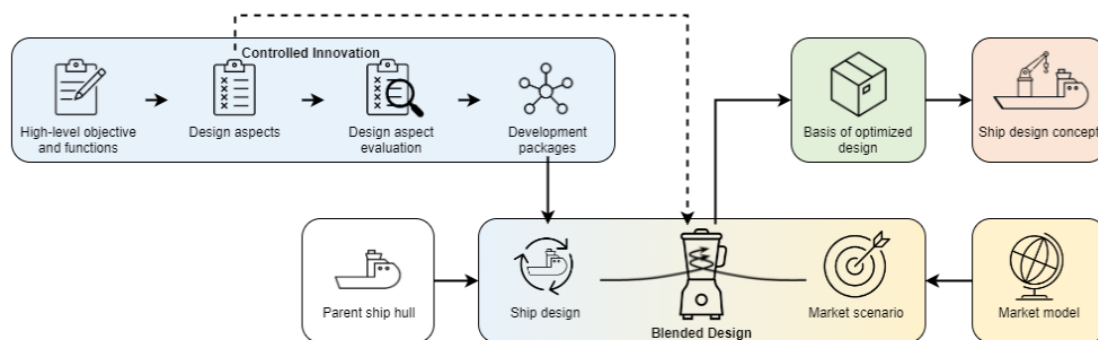


Figure 2: Schematic of the adopted design strategy for this research.

## High-level objective, Functions, and Design aspects

Following the CI process, first the high-level objective of Moonshot was determined, which is that the design should aim to be competitive in the offshore wind market and be efficient. Secondly, the functions to reach the objective were established, which are: hull shape requirements, mission equipment for wind turbine installation, payload, station keeping, motion performance, mobility, and accommodation. Then, the associated design aspects to these functions were determined. The identified design aspects are shown in the first column of Table 1. Arranging the design aspects revealed that there were a lot of unknowns for the design aspects, including requirements for ship particulars, type of lifting equipment, and the number of turbines Moonshot should carry per roundtrip. Also, properties of the cargo are unknown.

## Design aspects evaluation

Table 1 shows the design aspect evaluation, in which all design aspects are ranked. The first step involves assessing the level of the uncertainty of each requirement of a design aspects. Uncertainty in this context refers to the likelihood of changes in the requirements. Thereafter, the expected impact of an aspect on the ship design is determined. The two scores are then multiplied. Design aspects with higher scores indicate greater risks to the ship design. To decrease these risks, it is crucial to reduce uncertainty of the high-scoring design aspects and generate more knowledge to establish the right requirements with more certainty. Following CI, these high-risk design aspects are covered in detail in development packages. However, not all aspects will be covered solely in the development packages, as some will be addressed through Blended Design. The table shows the evaluation of the identified design aspects and indicates whether the path of development packages or Blended Design is proposed for high-scoring design aspects.

**Table 1: Evaluation of the design aspects.**

	Uncertainty 1 = certain 5 = uncertain	Consequence Design 1 = low impact 5 = high impact	Score Design Aspect $U \times C \times 0.2$	Assigned solution
<b>Hull shape requirements</b>				
Hull type	1	5	1.0	
Main dimensions	5	5	5.0	Blended design
<b>Mission equipment wind turbine installation</b>				
Installation method	2	5	2.0	
Lifting equipment	5	5	5.0	Development package
Lifting capacity	5	5	5.0	Blended design
<b>Payload</b>				
Type	1	4	0.8	
Size, mass and CoG of components	5	4	4.0	Development package and Blended design
Amount of turbines	5	5	5.0	Blended design
Deck cargo layout	4	4	3.2	Development package
<b>Station keeping</b>				
DP capability	2	4	1.6	
Operational area	1	3	0.6	
<b>Motion performance</b>				
Motion limits	5	3	3.0	
Workability	5	5	5.0	Blended design
<b>Mobility</b>				
Speed	4	5	4.0	Blended design
Mission	1	5	1.0	
<b>Accommodation</b>				
People on board	3	3	1.8	

## Development packages

Three design aspects were identified that should be covered in development packages to generate more knowledge, or before they can be incorporated in Blended Design, namely: the lifting equipment; the size, mass and CoG of components, and optimal deck layout.

### *Development package 1: Lifting equipment*

Since Moonshot will be a monohull and will install the turbine while floating, it will be susceptible to wave-induced motions. Therefore, the number of overboard lifts should be as low as possible to minimize risk. Therefore, the decision has been made to combine two installation methods to combine the benefits of those methods. The idea is to transport the turbine components separately, to allow for efficient use of deck space, and when at the installation location, assemble the turbine on board of the vessel. Then, the assembled turbine will be lifted overboard and installed on the turbine foundation. The right lifting equipment should be selected for this purpose. When looking at existing wind turbine installation vessels and future concepts, two types of vertical lifting mechanisms can be identified, free-hanging and guided (Figure 3).

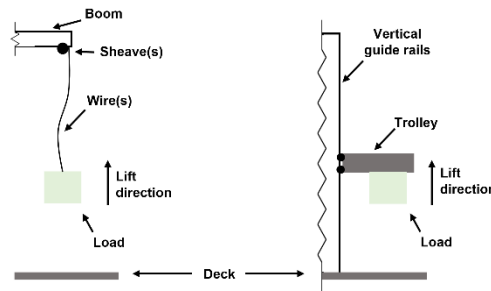


**Figure 3: Visualization of lifting mechanisms: free-hanging lift (left) and guided lift (right).**

The two mechanisms have been evaluated on the five aspects in Table 2. The main advantage of a guided lift mechanism would be to prevent swinging loads, minimizing the risk of damage to the turbine components. However, the main drawback of this mechanism would be that it would not be flexible and could not be used for other lifting purposes, because the working area of a guided lift system would be very small. Therefore, a hybrid solution between the two lifting mechanisms is preferred, a crane that can do both, such as the Zephyr crane by Huisman. Therefore, this lifting solution is adopted on the concept for Moonshot.

**Table 2: Assessment of the different lifting mechanisms, including a hybrid solution.**

	Free-hanging lift	Guided lift	Hybrid solution
Sufficient lifting capacity	Green	Green	Green
Prevention of swinging loads	Red	Green	Green
Stored position during transport	Green	Yellow	Green
Flexible	Green	Red	Green
Acceptable	Green	Yellow	Green

### **Development package 2: Size, mass, and CoG of components**

Information about the properties of next-generation offshore wind turbines is not available, resulting in uncertainty regarding the size, mass, and CoG of turbine components. To overcome this, an analysis into the properties of turbines has been conducted. A database was created with properties of 16 commercially available offshore turbine models of different sizes, and 7 generic reference offshore wind turbine models provided by research institutions. Spearman's rank correlation was used to determine the correlation between the various size and mass properties of the turbines. This showed that there is a strong correlation between all properties. The design of a wind turbine depends on the rated power, which is in turn linked to the squared rotor diameter (D). To understand the mass and size properties of turbines would scale with increased turbine capacity, scaling laws have been established with D as the independent variable. Two approaches, as described by (Sergiienko, et al 2022), were employed:

- 1) **Heuristic engineering fit** with  $y=cx^d+f$ , where x is the independent variable, and the exponent d is constant and based on expected geometric upscaling from physical laws or literature. Coefficients c and f are unknown, and f is non-zero for linear scaling;
- 2) **Best power fit** with  $y=ax^b$ , where coefficients a and b are unknown.

The coefficients were obtained by fitting curves, following the two approaches, through the data points from the wind turbine database. Then, the coefficient of determination ( $R^2$ ) was calculated to indicate how well the resulting curves fit the data. Eventually, the best fitting scaling law for each of the wind turbine properties has been established. These are shown in Table 3. When extrapolated, these can subsequently be used in Blended Design to estimate the size and mass of future turbine components. The center of gravity (CoG) location of the turbine components was estimated using literature and assumed for towers to be at 41% of the height (Quancard, et al 2019). The CoG of blades is located 35% from the blade root (Sørensen 1984) and for nacelles and hubs at the center of the components.

**Table 3: Scaling laws for each parameter based on a heuristic engineering approach and best power fit, based on the database with 23 offshore wind turbine models.**

Parameter	Heuristic engineering fit	R <sup>2</sup>	Best power fit	R <sup>2</sup>
$P_{rated}$	-	-	-	-
$D_{rotor}$	$5.98 \times 10^1 \cdot P_{rated}^{0.5}$	0.913	$6.02 \times 10^1 \cdot P_{rated}^{0.497}$	0.913
$L_{blade}$	$4.86 \times 10^{-1} \cdot D^1 + 0.113$	1.000	$4.89 \times 10^{-1} \cdot D^{0.999}$	1.000
$M_{blade}$	$1.16 \times 10^{-3} \cdot D^2$	0.903	$5.58 \times 10^{-3} \cdot D^{1.707}$	0.929
$L_{nacelle} + L_{hub}^*$	$8.23 \times 10^{-2} \cdot D^1 + 2.112$	0.819	$1.66 \times 10^{-1} \cdot D^{0.890}$	0.815
$B_{nacelle}^*$	$7.03 \times 10^{-2} \cdot D^1 - 4.433$	0.834	$1.47 \times 10^{-3} \cdot D^{1.658}$	0.882
$H_{nacelle}$	$6.13 \times 10^{-2} \cdot D^1 - 2.136$	0.719	$1.98 \times 10^{-2} \cdot D^{1.175}$	0.703
$M_{nacelle}$	$1.20 \times 10^{-2} \cdot D^2$	0.866	$1.59 \times 10^{-2} \cdot D^{1.947}$	0.867
$M_{hub}$	$2.76 \times 10^{-3} \cdot D^2$	0.584	$1.08 \times 10^{-3} \cdot D^{2.174}$	0.588
$L_{tower}$	$3.80 \times 10^{-1} \cdot D^1 + 39.328$	0.730	$4.27 \times 10^0 \cdot D^{0.622}$	0.735
$D_{tower}$	$3.89 \times 10^{-2} \cdot D^1 + 0.766$	0.888	$6.38 \times 10^{-2} \cdot D^{0.924}$	0.885
$M_{tower}$	$3.07 \times 10^{-2} \cdot D^2$	0.624	$5.89 \times 10^{-2} \cdot D^{1.880}$	0.626
$H_{hub}$	$4.68 \times 10^{-1} \cdot D^1 + 32.540$	0.822	$2.56 \times 10^0 \cdot D^{0.737}$	0.822

\*Only the direct and semi-direct drive turbines were used for this parameter.

### Development package 3: Deck layout

To investigate the optimal deck layout for Moonshot, eighteen different deck layouts were manually drawn with components for 15 MW turbines. The deck layouts differed with respect to crane, assembly, and installation location, as well as placement of the components on deck. Subsequently, all deck layouts were evaluated on the following aspects:

- Port logistics and transit
  - Loading
  - Transit
- Offshore operations
  - Tower lifting
  - Nacelle lifting
  - Blade lifting
  - Assembly lifting
- Capacity
  - Number of turbines
  - Efficient use of deck space
- Motion behavior
  - Assembly location
  - Installation location

An analysis was performed to establish local motions in the nacelle for two different loading conditions and at two different locations. The analysis was done for a case in the North Sea with a JONSWAP spectrum with  $\gamma=3.3$  at a significant wave height of 2.5 meters. The vessel was allowed to weathervane. For the analysis, software SESAM package by DNV was used. GeniE was used for creating a panel model, HydroD for modeling the environment and perform the hydrodynamic analysis in the frequency domain, using WADAM as a hydrodynamic solver.

All deck layouts were evaluated and scores on the various aspects were assigned. After evaluation, it was concluded that the best deck layout and crane position for Moonshot would be as shown in Figure 4.

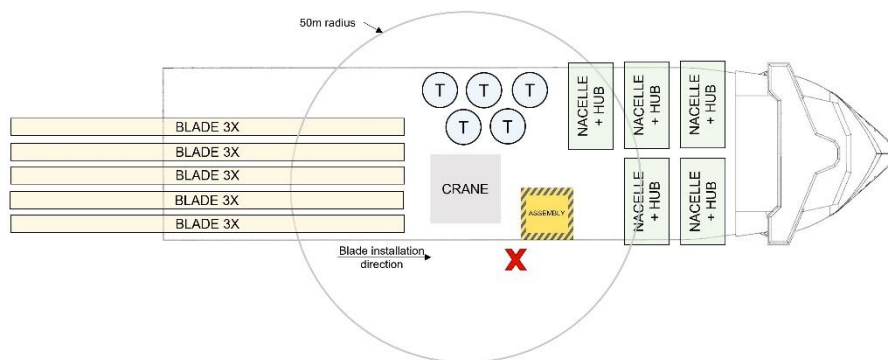


**Figure 4: The selected optimal deck layout for Moonshot.**

## BLENDED DESIGN FOR MOONSHOT

Blended Design is used to explore the design space of Moonshot and to elucidate the ship parameters based on financial and seakeeping performance. The existing model, as developed by Zwaginga (2020), Zwaginga et al (2021) generates a large number of unique design variations on a parent ship design by varying naval architectural parameters. For each of those design configurations, the lifetime financial performance is calculated within a simulated market environment. The model incorporates market uncertainty and different market scenarios can be considered to identify the optimal vessel size for evolving markets while balancing short- and long-term competitiveness. The current model could not directly be applied for the purpose of Moonshot as it cannot take into account seakeeping behavior and was originally designed for different vessel types, specifically heavy transport vessels (HTVs) and FIVs for monopile and jacket foundation T&I. In order to

adapt Blended Design for Moonshot, existing assumptions and functions needed to be updated or modified. Furthermore, new functionalities were added. Figure 5 visualizes the different parts of Blended Design and the connection between different functions of the entire model. The colors indicate what parts are added (green), unused (red), modified (blue), and left unchanged (white).

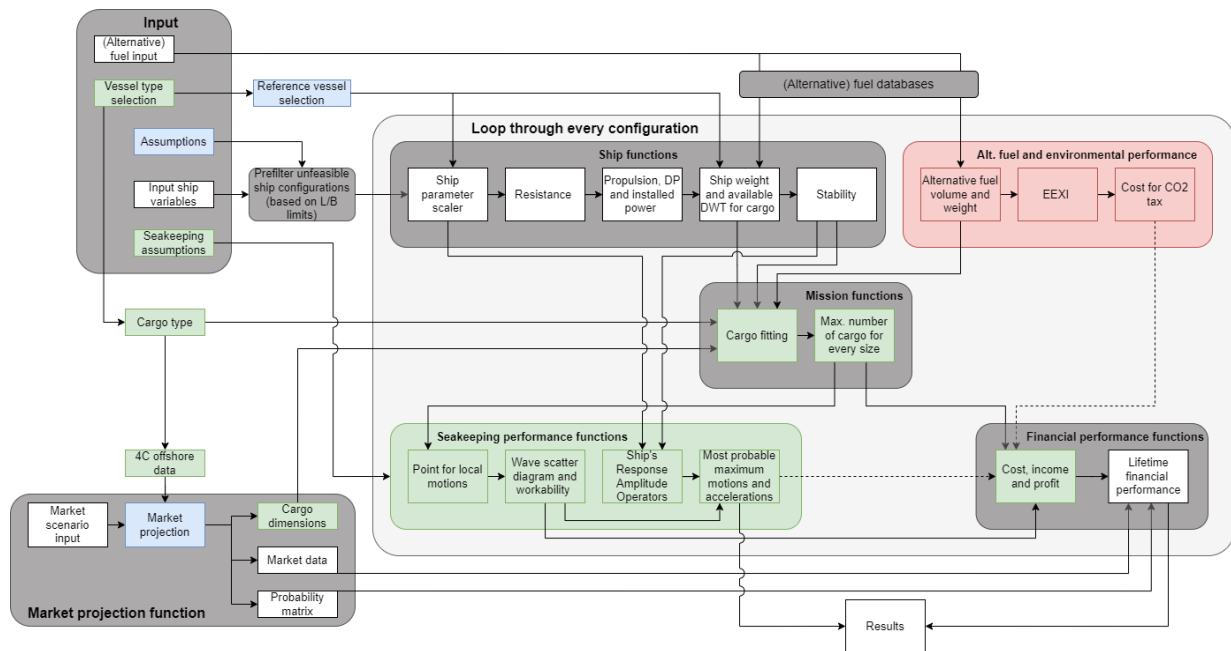


Figure 5: Integration of functions for Moonshot in Blended Design.

The biggest modifications to the model are the addition of the seakeeping performance functions and the mission functions for wind turbine components.

### Method for seakeeping analysis

Figure 6 presents the adopted approach for determining the seakeeping performance of every ship configuration in the design space. The output of this approach aims to provide the most probable maximum responses for the most-occurring sea state within the operational range of a vessel configuration. The operational range can be specified as input for Blended Design by setting a desired significant wave height ( $H_s$ ) limit. Based on the findings from the literature and market research, this limit was set to 2.5 meters for Moonshot.

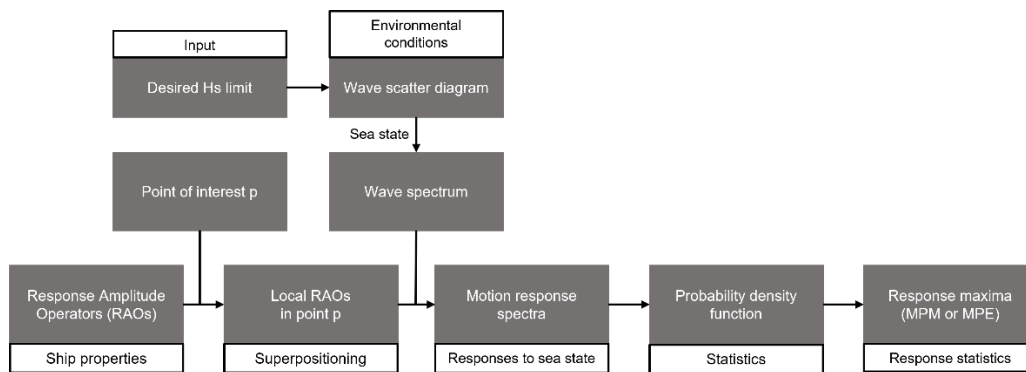


Figure 6: The approach to determine seakeeping behavior.

### Response Amplitude Operators

The main challenge with the approach is to determine the Response Amplitude Operators (RAOs) for all ship configurations within the design space. 2D Strip theory and 3D boundary element methods would not be applicable for the purpose of Blended Design, because these calculation methods would take too much time when calculating the RAOs for hundreds of thousands ship configurations. Furthermore, these methods require a hull-form geometry. However, this specific information is not available during the early-stage design and, as a result, not included in Blended Design. Therefore, a simpler method which only relies on ship parameters is needed. The paper by (Jensen, et al 2004) presents closed-form expressions (CFEs) to estimate the heave, roll, and pitch RAOs of a homogeneously loaded box by applying linear strip theory. To validate the method, RAOs were calculated for an UDSBV design of which RAOs computed with hydrodynamic analysis software (HAS) were available. The RAOs for different wave headings from the two methods were then compared. The visual validation revealed that the RAOs for the three motions, as calculated using the CFEs, appeared to be remarkably

similar. The trajectory of the RAOs calculated with the CFEs aligned with the behavior of the RAOs from HAS. The amplitudes of the motion RAOs appear to be around the same angular wave frequency, and the order of magnitude of the RAOs falls within the same range. Additionally, the area under each RAO curve was calculated and compared. The area is a measure of the transferred energy. This comparison is shown in Table 4.

**Table 4: Comparison of the areas under RAO curves for results from HAS and CFEs.**

		Wave heading angle										
Method		0°	15°	30°	45°	60°	90°	120°	135°	150°	165°	180°
Heave	HAS [s <sup>-1</sup> ]	0.41	0.42	0.44	0.48	0.57	0.93	0.61	0.51	0.46	0.43	0.42
	CFE [s <sup>-1</sup> ]	0.38	0.39	0.41	0.47	0.57	1.13	0.57	0.47	0.41	0.39	0.38
	<b>Error</b>	<b>-9%</b>	<b>-8%</b>	<b>-5%</b>	<b>-3%</b>	<b>1%</b>	<b>21%</b>	<b>-6%</b>	<b>-8%</b>	<b>-10%</b>	<b>-11%</b>	<b>-11%</b>
Roll	HAS [deg/ms]	0.00	0.24	0.49	0.72	0.93	1.11	0.90	0.70	0.48	0.24	0.00
	CFE [deg/ms]	0.00	0.19	0.41	0.66	0.97	2.04	0.97	0.66	0.41	0.19	0.00
	<b>Error</b>	<b>0%</b>	<b>-21%</b>	<b>-16%</b>	<b>-9%</b>	<b>4%</b>	<b>84%</b>	<b>8%</b>	<b>-5%</b>	<b>-14%</b>	<b>-20%</b>	<b>0%</b>
Pitch	HAS [deg/ms]	0.47	0.47	0.47	0.49	0.51	0.04	0.52	0.48	0.44	0.42	0.41
	CFE [deg/ms]	0.33	0.33	0.35	0.39	0.45	0.00	0.45	0.39	0.35	0.33	0.33
	<b>Error</b>	<b>-30%</b>	<b>-29%</b>	<b>-25%</b>	<b>-20%</b>	<b>-12%</b>	<b>-100%</b>	<b>-13%</b>	<b>-19%</b>	<b>-20%</b>	<b>-20%</b>	<b>-21%</b>

As displayed, the CFEs tend to underestimate the area under the RAO curves in comparison to the RAOs obtained from HAS. This implies that there is a difference in the total transferred energy across the entire range angular wave frequencies. The disparities between the two methods are most pronounced in beam seas. Also, a validation has been performed with another way to validate the RAOs from CFEs is to compare the standard deviation ( $\sigma$ ) of the resulting response spectra. This is because the distribution of the area under the RAO curves is also important to consider. Therefore, the differences in transferred energy do not provide the complete picture. To incorporate the distribution into the validation, response spectra were calculated for all RAOs in three different sea states with different wave peak periods ( $T_p$ ). A comparison for one of the periods is shown in Table 5.

**Table 5: Comparison of the standard deviation ( $\sigma$ ) of the response spectra at  $T_p = 7s$ , calculated using the RAOs from HAS and CFEs.**

		Wave heading angle										
Method		0°	15°	30°	45°	60°	90°	120°	135°	150°	165°	180°
Heave	HAS [m]	$5.8 \cdot 10^{-2}$	$5.7 \cdot 10^{-2}$	$5.9 \cdot 10^{-2}$	$6.8 \cdot 10^{-2}$	$8.0 \cdot 10^{-2}$	$3.9 \cdot 10^{-1}$	$1.1 \cdot 10^{-1}$	$8.8 \cdot 10^{-2}$	$7.3 \cdot 10^{-2}$	$6.5 \cdot 10^{-2}$	$6.3 \cdot 10^{-2}$
	CFE [m]	$4.2 \cdot 10^{-2}$	$4.4 \cdot 10^{-2}$	$4.9 \cdot 10^{-2}$	$7.2 \cdot 10^{-2}$	$8.4 \cdot 10^{-2}$	$5.7 \cdot 10^{-1}$	$8.4 \cdot 10^{-2}$	$7.2 \cdot 10^{-2}$	$4.9 \cdot 10^{-2}$	$4.4 \cdot 10^{-2}$	$4.2 \cdot 10^{-2}$
	<b>Error</b>	<b>-26%</b>	<b>-23%</b>	<b>-16%</b>	<b>7%</b>	<b>5%</b>	<b>46%</b>	<b>-21%</b>	<b>-18%</b>	<b>-32%</b>	<b>-32%</b>	<b>-32%</b>
Roll	HAS [deg]	0.0	$7.7 \cdot 10^{-4}$	$1.4 \cdot 10^{-3}$	$2.0 \cdot 10^{-3}$	$2.4 \cdot 10^{-3}$	$1.3 \cdot 10^{-3}$	$2.0 \cdot 10^{-3}$	$2.0 \cdot 10^{-3}$	$1.5 \cdot 10^{-3}$	$8.5 \cdot 10^{-4}$	0.0
	CFE [deg]	0.0	$3.2 \cdot 10^{-4}$	$7.2 \cdot 10^{-4}$	$1.2 \cdot 10^{-3}$	$2.0 \cdot 10^{-3}$	$1.1 \cdot 10^{-2}$	$2.0 \cdot 10^{-3}$	$1.2 \cdot 10^{-3}$	$7.2 \cdot 10^{-4}$	$3.2 \cdot 10^{-4}$	0.0
	<b>Error</b>	<b>0%</b>	<b>-59%</b>	<b>-49%</b>	<b>-38%</b>	<b>-17%</b>	<b>735%</b>	<b>-1%</b>	<b>-36%</b>	<b>-51%</b>	<b>-62%</b>	<b>0%</b>
Pitch	HAS [deg]	$2.5 \cdot 10^{-3}$	$2.5 \cdot 10^{-3}$	$2.6 \cdot 10^{-3}$	$3.0 \cdot 10^{-3}$	$5.0 \cdot 10^{-3}$	$4.7 \cdot 10^{-4}$	$5.1 \cdot 10^{-3}$	$2.9 \cdot 10^{-3}$	$2.3 \cdot 10^{-3}$	$2.0 \cdot 10^{-3}$	$1.9 \cdot 10^{-3}$
	CFE [deg]	$1.3 \cdot 10^{-3}$	$1.4 \cdot 10^{-3}$	$1.8 \cdot 10^{-3}$	$2.1 \cdot 10^{-3}$	$4.2 \cdot 10^{-3}$	0.0	$4.2 \cdot 10^{-3}$	$2.1 \cdot 10^{-3}$	$1.8 \cdot 10^{-3}$	$1.4 \cdot 10^{-3}$	$1.3 \cdot 10^{-3}$
	<b>Error</b>	<b>-46%</b>	<b>-42%</b>	<b>-32%</b>	<b>-29%</b>	<b>-15%</b>	<b>-100%</b>	<b>-17%</b>	<b>-27%</b>	<b>-22%</b>	<b>-28%</b>	<b>-30%</b>

The comparison showed that the error in the variances decreases as wave periods increase, or wave frequencies decrease. Overall, the variances from CFEs were lower than from HAS, but in the correct order of magnitude. Also, it is important to keep in mind the primary purpose of the method for determining the RAOs, which is to assess seakeeping behavior within Blended Design and predict the relative merits of various ship configurations. In this context, the method appears to be applicable. However, absolute results obtained from this method should be interpreted with caution.

### Local RAOs

RAOs are calculated in the CoG of a vessel. When linearizing for small motions, the independent RAOs can be translated to local motions in a point P through superposition. The phase angles of the RAOs are not known, so it is assumed for this research that the phases of all motions are such that the maximum motions occur at the same instance. This approach would yield the most conservative results. The resulting RAO in each of the three directions is then the sum of the associated RAOs in combination with the coordinates of point P with respect to the origin of the coordinate system, located at the CoG of the ship. For this project, point P will be located at the hub height in its installation position of the largest turbine every ship configuration can potentially carry in its lifetime in a specific market. This is visualized in Figure 7.

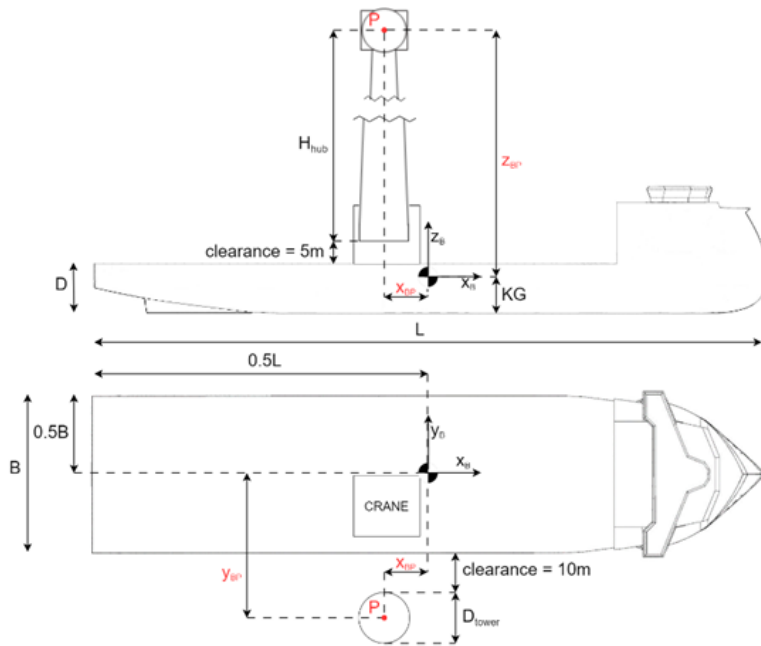


Figure 7: Schematic of the location of point P for local motions.

### Wave scatter diagram

A wave scatter diagram represents the joint probability of significant wave height ( $H_s$ ) and wave zero-up-crossing period ( $T_z$ ). The wave scatter diagram can be calculated for different worldwide locations and depends on multiple parameters. The values for those parameters have been derived using measurements and can be obtained from DNV-RP-C205 Environmental Conditions and Environmental Loads (Det Norske Veritas AS 2017). The seakeeping module is programmed such that different wave scatter diagrams can be considered, based on the input. For this research, zone 11 is used. The corresponding wave scatter diagram is presented in Figure 8.

When designing a vessel, it is common practice to aim for a certain workability or to set the limits up to which it can operate. Based on market research, it was decided that Moonshot should be able to operate up to  $H_s$  of 2.5 meters. This is highlighted by a black outline in the figure above and corresponds to a workability of more than 75 percent, which is acceptable. Of the sea states with a  $H_s$  of 2.5 meters, a  $T_z$  of 6.5 seconds is most occurring. For this research, this sea state (outlined in red) will be the sea state of interest.

Percent occurrence	$T_z$ [s]															Sum	
	0.5	1.5	2.5	3.5	4.5	5.5	6.5	7.5	8.5	9.5	10.5	11.5	12.5	13.5	14.5		15.5
0.5			0.467%	8.780%	14.052%	7.111%	1.972%	0.392%	0.064%	0.010%	0.001%						32.85%
1.5			0.009%	1.083%	6.704%	9.701%	6.324%	2.576%	0.786%	0.200%	0.045%	0.010%	0.002%				27.44%
2.5			0.133%	1.868%	5.036%	5.401%	3.321%	1.436%	0.493%	0.145%	0.039%	0.010%	0.002%	0.001%			17.89%
3.5				0.017%	0.447%	1.954%	3.071%	2.580%	1.449%	0.623%	0.223%	0.070%	0.020%	0.006%	0.001%		10.46%
4.5				0.002%	0.098%	0.650%	1.413%	1.544%	1.078%	0.557%	0.234%	0.085%	0.028%	0.008%	0.002%	0.001%	5.70%
5.5					0.020%	0.195%	0.567%	0.782%	0.662%	0.402%	0.194%	0.079%	0.029%	0.010%	0.003%	0.001%	2.94%
6.5					0.004%	0.054%	0.206%	0.352%	0.355%	0.250%	0.136%	0.062%	0.025%	0.009%	0.003%	0.001%	1.46%
7.5					0.001%	0.014%	0.069%	0.144%	0.172%	0.138%	0.085%	0.042%	0.018%	0.007%	0.003%	0.001%	0.69%
8.5						0.003%	0.022%	0.055%	0.076%	0.070%	0.048%	0.026%	0.012%	0.005%	0.002%	0.001%	0.32%
9.5						0.001%	0.006%	0.019%	0.032%	0.033%	0.025%	0.015%	0.008%	0.003%	0.001%		0.14%
10.5							0.002%	0.007%	0.012%	0.014%	0.012%	0.008%	0.004%	0.002%	0.001%		0.06%
11.5								0.002%	0.005%	0.006%	0.006%	0.004%	0.002%	0.001%	0.001%		0.03%
12.5								0.001%	0.002%	0.002%	0.002%	0.002%	0.001%	0.001%			0.01%
13.5									0.001%	0.001%	0.001%	0.001%	0.001%				0.00%
14.5																	0.00%
15.5																	0.00%
Sum	0.00%	0.00%	0.48%	10.02%	23.19%	24.72%	19.05%	11.77%	6.13%	2.80%	1.16%	0.44%	0.16%	0.05%	0.02%	0.00%	100%

Figure 8: Wave scatter diagram calculated for zone 11 (North Sea).

### Wave and response spectra

For this research, a JONSWAP wave spectrum will be used with a peak enhancement factor ( $\gamma$ ) of 3.3. The wave spectrum will be calculated for the sea state of interest for the specified zone in Blended Design, as explained earlier. After the wave spectrum is determined, the response spectra for each of the motion directions and wave headings can be established. The motion response spectrum describes the response to waves of a floating body at different wave frequencies.

### Response maxima

To assess the seakeeping characteristics of the ship configurations, it is important to predict the highest response value within an irregular sea state within a certain time. This is done with probability distributions. A good approximation for the distribution of response maxima can be obtained using a Rice distribution function. This probability distribution depends on the variance ( $\sigma_s$ ) of the response spectrum and spectral width parameter ( $\epsilon$ ). When the  $\epsilon=0$ , the Rice distribution reduces to the Rayleigh distribution. For  $\epsilon \leq 0.9$ , the most probable largest value in  $n$  observations of a random process, as given in (Bhattacharya 1973), is calculated by Equation 1 and 2.

$$n = \frac{T}{T_z} \quad [1]$$

$$\eta_n = \sigma_s \left[ 2 \ln \left( \frac{2\sqrt{1-\epsilon^2}}{1+\sqrt{1+\epsilon^2}} \cdot \frac{n}{\alpha} \right) \right]^{1/2} \quad [2]$$

The most probable largest value  $\eta_n$  depends on a risk factor  $\alpha$ . This factor is the probability that the extreme value will exceed  $\eta_n$ . For example, for  $\alpha=1$ , the most probable maximum (MPM) value is calculated. This is the most-likely maximum response that will occur within the specified time interval  $T$ . This interval is commonly 3 hours. The MPM response value typically has a 63 percent probability of being exceeded. On the other hand, with  $\alpha=0.01$ , the exceedance probability is only 1 percent, which is often referred to as the most probable extreme (MPE) response. An example of a probability density function (PDF) and cumulative distribution function (CDF) for  $n$  response observations is depicted in Figure 9. Also, the MPM and MPE values with an  $\alpha$  of respectively 1.0 and 0.01 are shown.

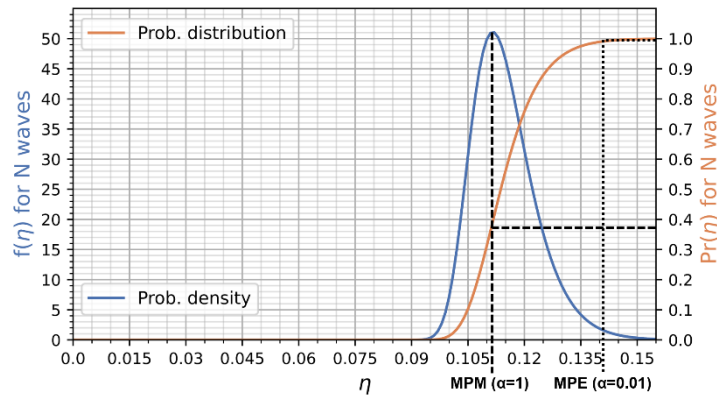


**Figure 9: Rayleigh PDF and CDF ( $\epsilon = 0$ ) for  $m_0 = 8.02 \cdot 10^{-4}$  and  $n=2,207$  waves ( $T_p=5.5s$ ).**

The decision of the value for  $\alpha$  depends on the acceptable risks and designer's decision. When looking at the MPM and MPE responses of the CDF above, it stands out that the difference between the two values is relatively low, respectively 0.114 and 0.142 meters. This depends on the steepness of the CDF and is thus directly related to the properties of the response spectrum. It should be noted that the response spectrum will be different for every wave heading, ship motion direction, and sea state. Therefore, the MPM and MPE values of other cases might be further apart, and when interpreting the results, it is important to keep in mind that the results are based on statistics and larger responses could occur. Thus, for this research, the decision was made to calculate the MPE ( $\alpha = 0.01$ ) responses, representing a more conservative approach. The calculation of MPE response values is executed for every wave heading. Ultimately, the MPE responses across the three directions (x,y,z) for all wave headings are determined. With these results, the worst MPE responses across the longitudinal, transverse, and vertical direction can be determined for every ship configuration.

### Validation of the module

To validate the output of the seakeeping module, the worst local MPE motion responses were calculated for an UDSBV design. These results were compared to the results from HAS under the same conditions as used in the module. The results were calculated for two different loading conditions, at both the assembly and installation position of the turbines, and for different sea states. Also, the validation was conducted for both a weathervaning and omnidirectional condition. The results demonstrated that the local MPE displacement of the two methods are comparable and within the same order of magnitude in the weathervaning condition. One of the validations, for  $T_p=6.2s$  is shown in Table 6.

**Table 6: Validation of weathervaning MPE motion-induced displacements from the seakeeping analysis module (SAM) with hydrodynamic analysis software (HAS).**

Position		Most probable extreme					
		Fully-loaded			Lifting last turbine		
		Long. disp. [m]	Trans. disp. [m]	Vert. disp. [m]	Long. disp. [m]	Trans. disp. [m]	Vert. disp. [m]
Assembly location	HAS	0.77	0.15	0.26	0.94	0.25	0.32
	SAM	0.74	0.22	0.21	0.74	0.27	0.21
	Error	-4%	44%	-21%	-21%	10%	-33%
Installation location	HAS	0.84	0.15	0.27	1.01	0.25	0.32
	SAM	0.74	0.22	0.23	0.74	0.27	0.25
	Error	-11%	44%	-14%	-26%	10%	-24%

However, minor differences were observed, especially in longitudinal motion direction. This is likely because the simplified method does not consider coupling effects between motions and probably the omission of three of the six RAOs

does play a minor role. However, for the purpose of this research, the outcomes of the new module are considered acceptable. The validation of the omnidirectional condition showed that this method cannot be used for this type of environment. This is mainly a result of the large discrepancies in the RAOs in beam seas.

### Wind turbine mission module

The wind turbine mission module connects the wind turbine market within Blended Design with the ship configurations. The module determines the feasible number of turbines that can be transported and installed by each ship configurations. Given the diversity of turbine sizes in a market, this calculation is performed for every possible turbine size. The number of turbines is dependent on multiple constraints. The module calculates the number of turbines a ship configuration can carry for each of the constraints and then identifies the limiting factor that yields the smallest number of turbines that can be transported and installed. This procedure is depicted in Equation 3.

$$N = \min\{N_{CC}, N_A, N_{DWT}, N_{tot,tr}, N_{tot,lift}\} \quad [3]$$

### Crane capacity constraint

The crane capacity of a ship configuration determines the maximum turbine weight that can be lifted, (see Equation 4).

$$N_{cc} = \begin{cases} \infty, & \text{if } m_{WTG} < \text{crane capacity} \\ 0, & \text{else} \end{cases} \quad [4]$$

### Deck area constraint

The number of turbines for different sizes, that could fit in the free deck space of a configuration is calculated. For the analysis, the deck area is divided into two parts (see Figure 10). It is assumed that the green area will be reserved for towers and nacelles with hubs. The yellow area, behind the crane, is designated for blade storage. White areas cannot be used.

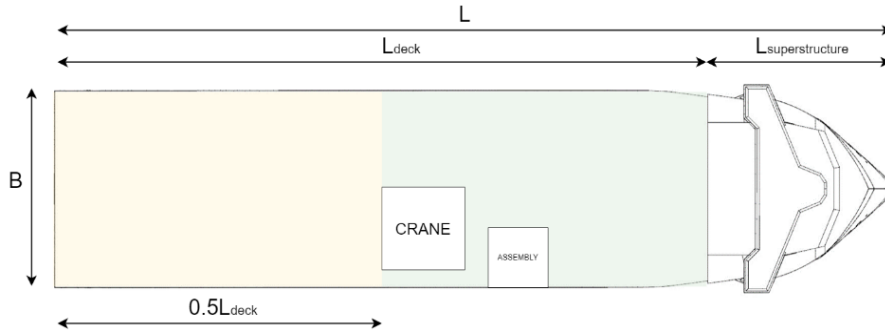


**Figure 10: Division of deck area.**

The dimensions originate from the results from development package 2. To account for seafastening and ensure sufficient spacing, a margin of 1 meter around the nacelles is assumed. For towers, a square footprint of the tower diameter with an offset of 1 meter on each side is assumed. To account for unused space, a margin of 90 percent is adopted. The number of turbines, with this margin included, was found to better match realistic deck layouts. The number of turbines, based on towers and nacelles fitting in the green area is calculated according to Equation 5.

$$N_{A,1} = 0.9 \cdot A_{deck,green} / [(L_{nacelle} + 2) \cdot (B_{nacelle} + 2) + (D_{tower} + 2)^2] \quad [5]$$

Afterwards, the number of blades that fit within the width of the yellow part is calculated. Blades are assumed to be stacked in blade racks in pairs of three. The algorithm checks whether the width of all blade stacks does not exceed the breadth of the vessel and automatically adjusts the number of turbines if that is the case. This is depicted in Equation 6.

$$N_{A,2} = \begin{cases} B / (B_{blade} + 2), & \text{if } N_{A,1} \cdot (B_{blade} + 2) > B \\ N_{A,1}, & \text{else} \end{cases} \quad [6]$$

Based on the deck layout, blades are assumed to extend over the aft of the vessel. The estimated length that should fit on the length of the yellow part of the deck is set at 60 percent of the total blade length. A check is performed to verify if this requirement is satisfied. A margin of 5 meters between the aft of the crane and blade racks is assumed (Equation 7).

$$N_A = \begin{cases} N_{A,2}, & \text{if } 0.5L_{deck} - 5 \geq 0.6L_{blade} \\ 0, & \text{else} \end{cases} \quad [7]$$

### Deadweight constraint

The third limiting factor is associated with the deadweight available for cargo. The algorithm calculates the maximum number of turbines that can be accommodated within the vessel's deadweight. This calculation assumes that there is no ballast water used. The total mass of a single turbine is defined in Equation 8.

$$m_{WTG} = m_{tower} + m_{nacelle} + m_{hub} + 3 \cdot m_{blade} \quad [8]$$

The number of turbines is calculated using Equation 9. An allowance of 10 percent is assumed for the mass of seafastening.

$$N_{DWT} = DWT / (1.1 \cdot m_{WTG}) \quad [9]$$

### Transit and lifting stability constraints

Blended Design calculates the maximum allowable KG value for both transit and lifting conditions of all ship configurations. Within the turbine mission module, the vertical center of gravity (VCG) for an increasing number of wind turbines of every size in the market simulation is calculated. It then checks if the VCG of the turbines is still below the allowable KG. If not, the vessel will be unstable and not be able to carry that number of wind turbines. The algorithm eventually finds the maximum number of wind turbines for which the KG value is still positive. Ballast water is incorporated in both cases. The VCG of ballast water is a fixed ratio of the depth. The mass of ballast water is calculated following Equation 10.

$$m_{bal} = DWT - N_{WTG} \cdot m_{WTG} \quad [10]$$

The VCG of the turbine components corresponds with the findings from development package 2. To determine the resulting VCG of these components, when they are in storage position on deck during transit, Equation 11 is used.

$$VCG_{comp} = D + \frac{3m_{blade} \cdot 0.5 \cdot 3h_{blade} + m_{tower} \cdot VCG_{tower} + (m_{nacelle} + m_{hub}) \cdot VCG_{nacelle}}{m_{turbine}} \quad [11]$$

The VCG of the deck cargo in transit and lifting condition is then calculated with the following Equations 12 and 13.

$$VCG_{tr} = \frac{VCG_{LSW} \cdot LSW + N_{tot,tr} \cdot VCG_{comp} \cdot m_{WTG} + VCG_{bal} \cdot D \cdot m_{bal,tr}}{\Delta_{tr}} \quad [12]$$

$$VCG_{lift} = \frac{VCG_{LSW} \cdot LSW + (N_{tot,lift} - 1) \cdot VCG_{comp} \cdot m_{WTG} + VCG_{bal} \cdot D \cdot m_{bal,lift} + z_{load} \cdot m_{WTG}}{\Delta_{lift}} \quad [13]$$

### Validation

The module has been validated using a reference vessel from UDSBV. Validation has been performed for 8, 15, and 20 MW turbines. Deck layout drawings were made, and calculations were done to check whether the calculated number of turbines for every constraint for the different turbine sizes matches. The results were found to be the same, so it is assumed that the wind turbine mission module produces sensible results.

## EVALUATING THE PERFORMANCE OF MOONSHOT

After the new modules were created and adaptations to Blended Design were made, the design space is explored to evaluate the performance of different ship configurations and to elucidate optimal design parameters for next phases of the design. Firstly, a design space was created by varying ship parameters. In total, the design space consisted of 158,340 unique ship configurations, as displayed in Table 7.

**Table 7: The created design space in Blended Design.**

Particular	Start	End	Step size	#
Length [m]	140.0	280.0	5.0	29
Breadth [m]	36.0	72.0	3.0	13
Depth [m]	10.0	19.0	1.0	10
Sailing speed [kn]	10.0	15.0	1.0	6
Crane capacity [t]	1,000	7,000	1,000	7
Block coefficient [-]	0.77	-	-	1
<b>Unique configurations</b>				<b>158,340</b>

The output from Blended Design is visualized in graphs that show the performance of all configurations for a specific ship parameter. A Pareto front is drawn through the best-performing configurations for every parameter. Figure 11 depicts the visualization of the how the resulting graph is constructed and how to interpret it. The optimal range is user-defined and is set to 2.5 percent for this research.

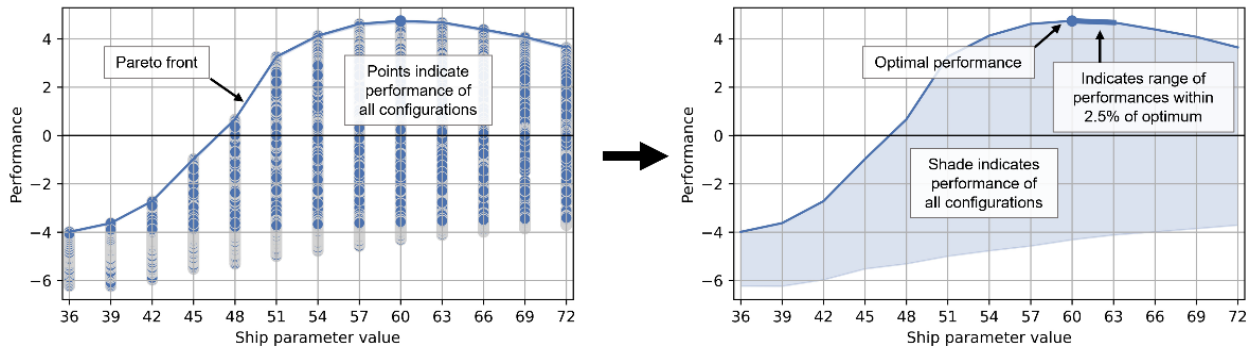


**Figure 11: Visual guide on how to interpret the result plots.**

Firstly, the results from the financial performance analysis of all configurations within the design space is discussed. Secondly, the seakeeping performance will be presented.

### Financial performance

The influence of ship parameters on the financial performance has been investigated. Different scenarios have been incorporated in the analysis and optimal design ranges have been determined. The financial performance is measured in return on investment (ROI), which is the ratio between the net profit over the lifetime and the investment costs. The revenue of each ship configuration consists of an installation reward per installed MW. Thus, every vessel will be rewarded for the number of turbines and size of turbines it installs.

#### Performance in different market scenarios

Figure 12 presents the financial performance in four different future markets. The unbound market assumes that the turbine growth is not limited. The 16MW bound market assumes that the turbines will not grow beyond the maximum turbine capacity of all offshore wind projects currently in operation, planned or within the Procurement, Construction, and Installation (EPCI) phase. The 1,000 feet bound market assumes that the growth of turbines is restricted to a tip height of 1,000 feet. This scenario has recently been proposed by the Netherlands Wind Energy Association (NWEA) (Rijntalder 2023). The maximum rotor diameter in this case would be around 280 meters (Netherlands Wind Energy Association 2023), which would correspond to a 22MW turbine. Once this capacity is reached, the size of turbine components is assumed to not further increase. Uncertainty in the mass of components is only considered in the third scenario. In the fourth scenario, the market would be bound to 22MW, but uncertainty in both the size and mass properties is considered. The difference in optimal design parameters for different market scenarios is clearly visible.

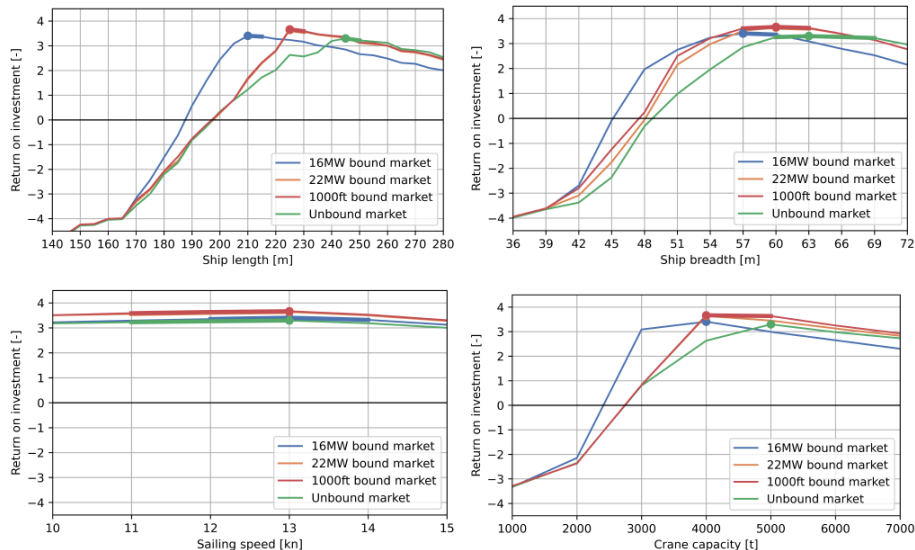


**Figure 12: Visualization of the results for the four market scenarios.**

#### Influence of distance to port

Figure 13 presents the financial results for different distances between the OWFs and marshalling ports. The calculations for the different market scenarios were conducted with a distance of 140 nautical miles (NM). This distance was selected based on insights from literature, as it corresponds to the anticipated maximum distance to shore for future OWFs in 2026 (NORWEP 2022). To explore the impact of varying distance ranges, both shorter and longer distances were included. The short distance of 35 NM is based on current global maximum distances from (NORWEP 2022). The long distance is ten times that distance. The distance to port effects the ROI of different configurations. This is mainly due to the increasing

sailing distance, decreasing the number of turbines that can be installed. Larger vessels perform better as distance increases, which can be attributed to the increased cargo capacity, ensuring that they can take more turbines per roundtrip. The optimal sailing speed is the same for all distances, but the optimal range narrows down as distances increase, favoring faster configurations at large sailing distances.

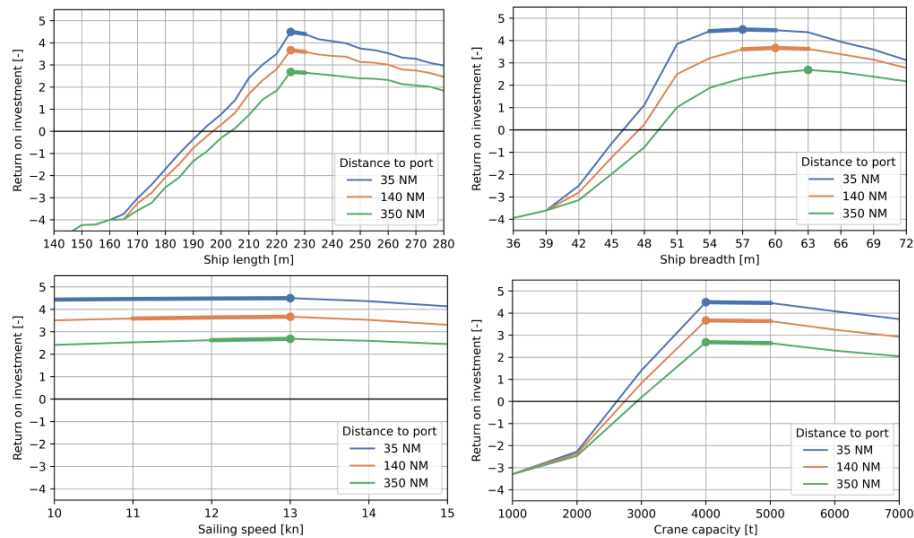


Figure 13: Visualization of the results of a 1,000ft bound market with three distances to port.

### Influence of splitting the turbine towers

The turbine towers are assumed to be transported vertically and as one part. The towers are very heavy and tall, resulting in high VCGs. The number of turbines a ship configuration can transport and install could be constrained by five different limiting factors, including stability. Therefore, an analysis was conducted on the distribution of limiting factors across all feasible ship configuration, to gain insight in what drives the carrying capacity. Figure 14 presents a breakdown of the limiting factors for all feasible ship configuration and a distribution with distinction per turbine size.

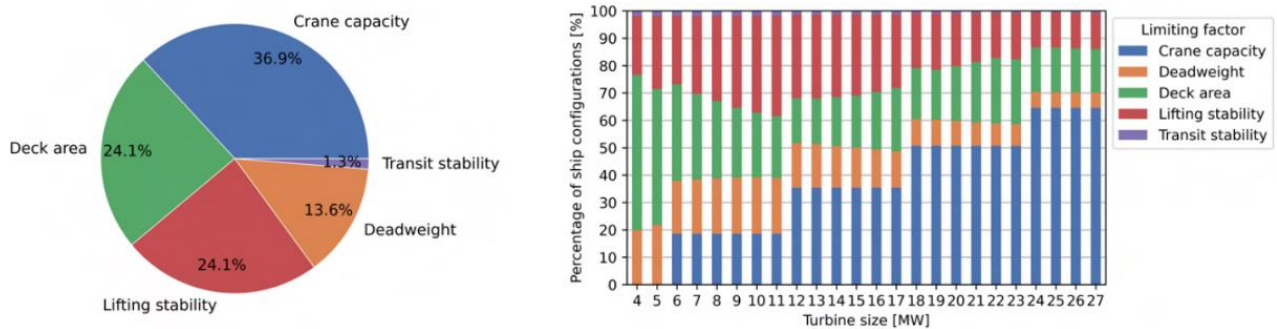
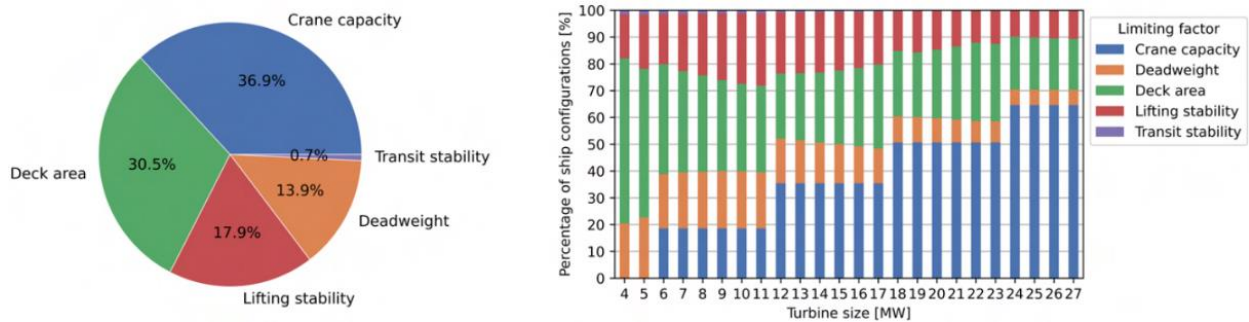


Figure 14: Distribution of limiting factors for ship configurations (left) and aggregated per turbine size (right).

In most ship configurations, the limiting factor is the crane capacity. This is because the design space consists of configurations with crane capacities ranging from 1,000 to 7,000. As turbine size increases, crane capacity becomes more limiting. After that, deck area and lifting stability are the most limiting constraints. The fact that many configurations is limited by lifting stability, indicates that the deck area or deadweight, and thus the full potential of a lot of ship configurations is not completely used. The main reason why lifting stability is limiting in a lot of configurations is because of the high VCG of the turbine towers.

This led to investigating the effects of transporting the turbine towers as two smaller parts, rather than one large components. Splitting the towers in two parts would benefit the overall VCG of the turbine components. On the other hand, more deck area would be needed to transport one tower and more lifts would have to be performed when loading and installing the towers, doubling loading and installation times for tower parts. Figure 15 depicts how the limiting factors are distributed across the carrying capacity of all feasible ship configurations when the towers are transported as two parts.



**Figure 15: Distribution of limiting factors for ship configurations (left) and aggregated per turbine size (right) with towers transported as two parts.**

As shown in the figures above, the lifting stability constraint is a less dominant limiting factor for the carrying capacity of wind turbines. The share of the deck area limiting factor among all configurations has significantly been increased. This shift suggests that the carrying capacity of the ships is used more efficiently. The difference in carrying capacity when the tower is divided into two parts, for one of the configurations in the design space is visualized in Figure 16. The two plots depict the number of turbines that can be transported according to the five constraints for every turbine size. It also shows the main limiting factor for every turbine size and the resulting capacity.

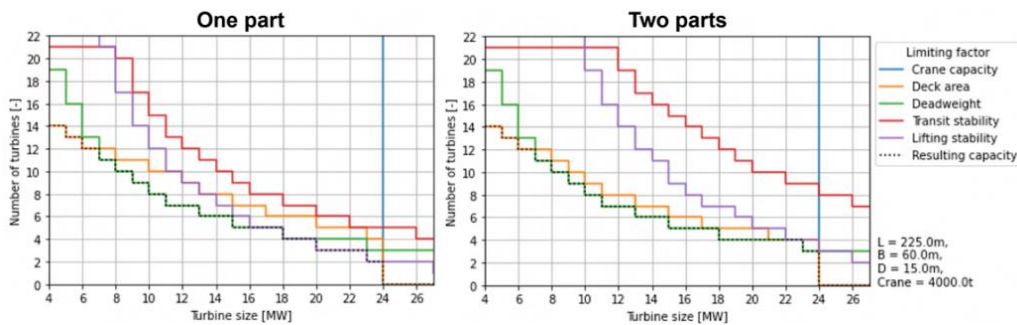


**Figure 16: Visualization of limiting factors and number of turbines for the two tower strategies.**

To assess the benefits of the transportation strategy, a financial performance analysis was conducted. The goal is to determine whether the advantages of transporting the towers as two parts outweighs the negative consequences. The financial performance is depicted in Figure 17. As visible, the ROI of all configurations is lower when the towers are divided into two parts instead of being transported as single components with a high VCG. Therefore, it can be concluded that there is no financial benefit in carrying the towers as two parts.

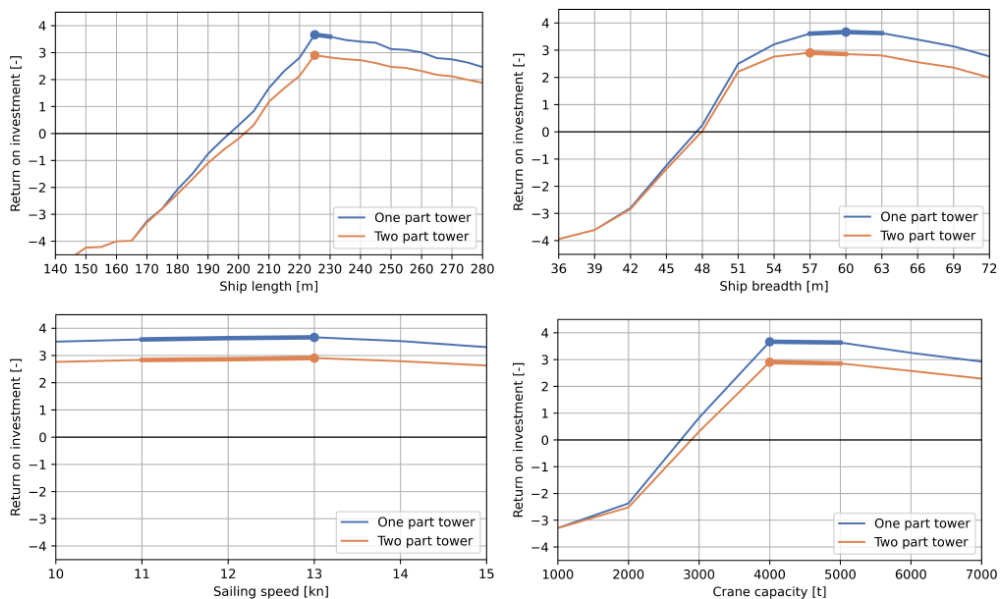


**Figure 17: Visualization of the results for two different tower transportation strategies in a 1,000ft bound market. The distance to port is 140 NM.**

## Seakeeping performance

The influence of various ship parameters will be investigated, and optimal design configurations will be determined for best seakeeping performance. The calculations have been performed for a significant wave height of 2.5 meters. The performance is measured in local MPE responses, as explained earlier. The lower the responses, the better. The local responses are calculated at the hub height of the largest turbine a ship configuration can possibly transport and install during its lifetime. This is during offshore operations, so when the vessel is station keeping. The ship is assumed to weathervane, meaning that it is allowed to align the bow with the incoming environment. This improves seakeeping and reduces the power required for dynamic positioning. While weathervaning, the environment is assumed to be at 180 degrees with an offset of 30 degrees to both sides, as visualized in Figure 18.

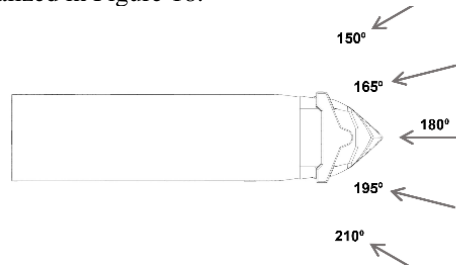


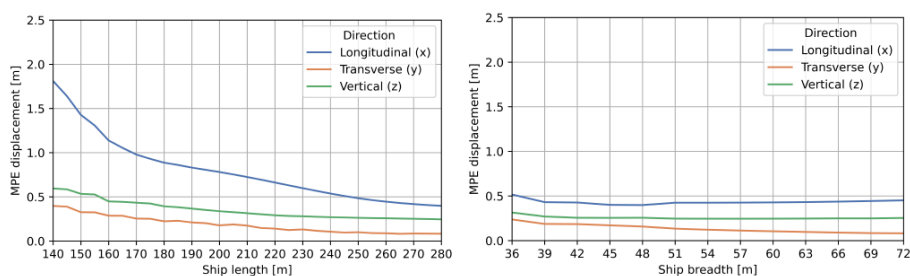
**Figure 18: Wave headings during weathervaning with an allowed offset of  $\pm 30$  degrees.**

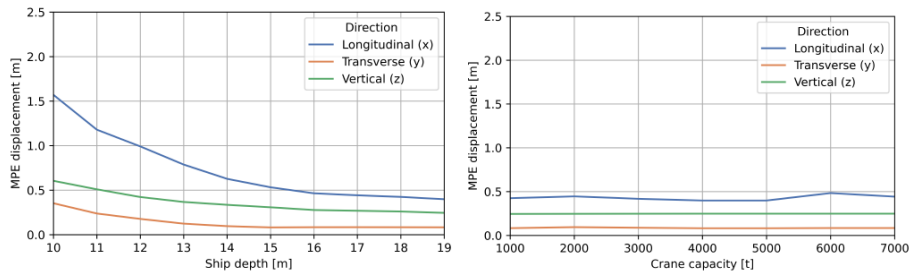
### *Weathervaning displacements*

Figure 19 shows the MPE motion-induced displacements in each of the three motion directions for different ship parameters. The results reveal that the longitudinal motion response is most dominant. This can be attributed to the environment while weathervaning, where waves are primarily coming in at the bow of the vessel. The main contributor to the longitudinal response is the pitch motion, which is lower for increasing ship lengths. Increasing the breadth does not really influence the MPE motion responses. In transverse direction, the main contributor to the motion displacement is the roll motion. However, roll motion is quite low due to the weathervaning and the used method for determining the RAOs. The used method neglects coupling effect between motions, disregarding for example roll motion due to pitch. Regarding vertical direction, the foremost contributor to the motion displacement is the heave motion in combination with pitch and roll. The results show that the vertical motion decreases for longer ships. This could be because the heave motion RAO shift to lower wave frequencies for longer ship. This results in lower RAO values at the same wave frequency for longer ships. When looking at breadth, relatively constant lines are observed. This is because heave motion is not significantly influenced by ship breadth with the used calculation method. In addition, due to decoupled motions and the weathervaning, the roll motion is also very little influenced by increased breadth.

The influence of depth on the motion behavior of configurations is not straightforward. As depth increases, so does the maximum draft of a configuration, leading to an increase in displacement, which affects the motion behavior. However, an increase in draft leads to a decrease in sectional hydrodynamic damping ( $A$ ) and the Smith correction factor ( $\kappa$ ) in the method from (Jensen, et al 2004), influencing the forcing functions for heave ( $F_3$ ) and pitch ( $F_5$ ), subsequently affecting heave and pitch RAOs. Additionally, increasing depth and draft affect stability in several ways. Draft affects the  $GM_T$  value of a ship configuration, impacting stability and the behavior of the roll RAO. An increase in depth at the same breadth reduces the B/D ratio, crucial for establishing the GZ curve, which determines the transverse stability. Stability influences the maximum turbine size the configurations can transport and install and, consequently, dictating point P in which local responses are calculated. In general, increasing depth results in decreased MPE motion displacement in all directions, as reflected in Figure 19.

Crane capacity has limited influence on motion behavior. The lines for all three directions remain relatively constant because the best ship configurations with optimal motion behavior are independent of crane capacity. For instance, the 'best' configurations for longitudinal motions have low to moderate breadth and the highest depth, providing the best motion behavior in the longitudinal direction. But due to their low B/D ratio resulting from the combination of breadth and depth, their stability is typically poorer, limiting their ability to handle larger turbine sizes in the market. For these smaller sizes, the point P where motions are calculated is closer to the CoG of the vessel, resulting in lower longitudinal motions.





**Figure 19: Wave headings during weathervaning with an allowed offset of +30 degrees.**

The model behavior explained above is not the most elegant way to design a vessel, but the model does achieve the objective of finding the configurations with the best seakeeping behavior. This model behavior, while effective, can be considered undesired and should be considered when evaluating motion behavior or optimizing a vessel on motion performance.

Figure 20 presents a parallel coordinates plot of the motion performance. The plot shows all possible configurations with their MPE motion responses in all three directions. Three combinations of ship parameters have been highlighted. These three configurations would have the lowest MPE displacement for one of the three directions. These three optimal ships would be very large, with the smallest crane possible. The model selects these configurations as the best one, because it can only lift the smallest turbines, with point P for motion calculation closest to the CoG of the vessel. Considering the findings from financial performance and the best configuration in terms of motion performance, a large gap between the best ship configuration for Moonshot is found. This gap will be addressed later.

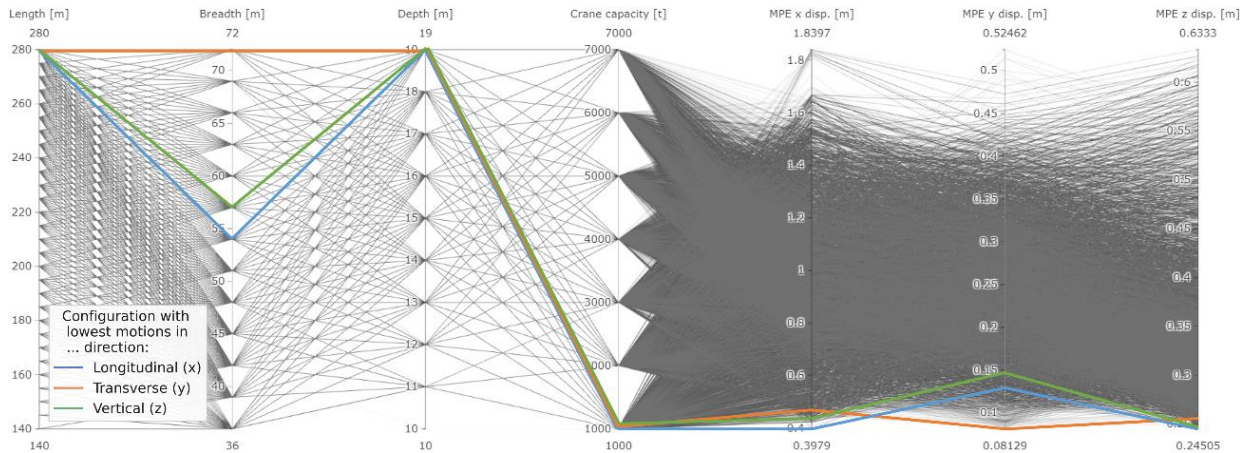


**Figure 20: Parallel coordinates plot of motion performance.**

### ***Weathervaning accelerations***

The accelerations during weathervaning have also been evaluated. Just as the MPE displacements, the MPE accelerations were also calculated in point P for the three directions. These three components were then translated to a resultant MPE acceleration vector using Equation 14.

$$MPE \mathbf{a} = \sqrt{(MPE \mathbf{a}_x)^2 + (MPE \mathbf{a}_y)^2 + (MPE \mathbf{a}_z)^2} \quad [14]$$

Figure 21 depicts the resulting MPE acceleration vector in relation to displacement of all configurations. To prevent damage to wind turbines, suppliers prescribe limits on acceleration in the nacelle during T&I. The acceleration limit is typically 0.5g (~4.9 m/s<sup>2</sup>) (BVG Associates 2019). As demonstrated in the figure, the local MPE acceleration for all configurations remains well below this specified limit. Consequently, accelerations in the nacelle are not deemed to be a major concern.

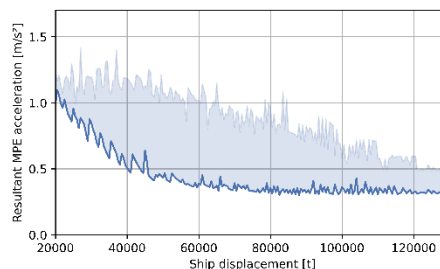


**Figure 21: Visualization of the MPE acceleration vector results.**

## Combining seakeeping and financial performance

As previously highlighted, conflicting optimal ship configurations emerge when optimizing for either financial performance or seakeeping performance. To reconcile this discrepancy between the two objectives, a financial penalty will be imposed on configurations exhibiting inferior seakeeping behavior. This penalty will be in the form of an added cost for motion compensation, which is a supplement to the base cost for the main crane. The unit of this metric is €/t.m), encompassing both the crane capacity and the cumulative MPE displacement in longitudinal, transverse, and vertical direction, measured in meters. While the metric might not be documented in existing literature, it aligns well with practical considerations. It is reasonable to expect that cost of lifting equipment would increase with increasing motion compensation requirements. Moreover, the inclusion of crane capacity in the metric is also logical, as a motion compensation system for higher crane capacity would likely be more complex and larger, inherently being more expensive.

As this metric is not documented in existing literature, there is no reference for quantifying the cost of motion compensation. Consequently, a range with different cost levels has been assumed. This range spans from €0 to €10,000/(t.m). The resulting ROI for these different cost levels is depicted for different ship parameters in Figure 22. As displayed, the ROI decreases for increasing cost levels for motion compensation. What stands out, is that the optimum for length shifts to longer configurations. This indicates that at a certain point, the higher cost of investing in and operating a longer ship surpasses the increased cost for motion compensation of shorter vessels.

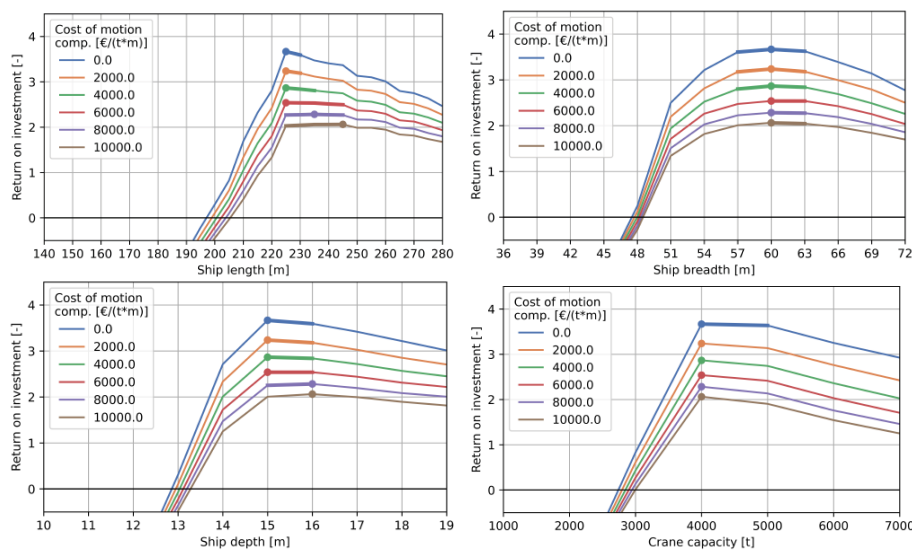


Figure 22: Visualization of the financial results with motion performance penalty in a 1,000ft bound market with an operational  $H_s$  limit of 2.5 meters.

## Optimal design ranges for Moonshot

Considering all findings, optimum design ranges for the ship have been established. These findings for different scenarios are summarized in Table 8. The initial design parameters can be chosen according to client preferences or based on a designer's perspective. The initial design parameters, as chosen by the author, are displayed in the last row of the table.

Table 8: Summary of optimal design parameters for Moonshot.

Scenario	Length [m]	Breadth [m]	Depth [m]	Sailing speed [kn]	Crane capacity [t]
<b>Financial performance</b>					
16MW bound market	210-215	57-60	14-15	12-14	4,000
22MW bound market	225-230	60-63	15	11-13	4,000
1,000ft bound market	225-230	57-63	15-16	11-13	4,000-5,000
Unbound market	245-250	60-69	16-17	11-13	5,000
<b>Distance to port<sup>+</sup></b>					
35 NM	225-230	54-60	15	10-13	4,000-5,000
140 NM	225-230	57-63	15-16	11-13	4,000-5,000
350 NM	225-230	63	16	12-13	4,000-5,000
<b>Seakeeping performance<sup>+*</sup></b>					
Weathervaning x-displacement	280	54	19	11-13	1,000
Weathervaning y-displacement	280	72	19	11-13	1,000
Weathervaning z-displacement	280	57	19	11-13	1,000
<b>Motion compensation<sup>+*</sup></b>					
€2,000/(t.m)	225-230	57-63	15-16	11-13	4,000
€6,000/(t.m)	225-245	60-63	15-16	11-13	4,000
€10,000/(t.m)	225-245	60-63	16	11-13	4,000
<b>Initial design parameters</b>	<b>230</b>	<b>63</b>	<b>16</b>	<b>12</b>	<b>4,000</b>

\* in a 1,000ft bound market with a 140 NM distance between port and OWF. ° for a maximum significant wave height of 2.5 meters. + in a 1,000ft bound market scenario.

## BENCHMARKING THE DESIGN

Previous results indicate that the Moonshot could be a viable alternative for offshore wind turbine installation. However, the question arises whether it measures up against existing technologies. To benchmark, a version of Moonshot has been designed to directly compete with the largest jack-up design in the market, the NG-20000X (GustoMSC n.d.). This jack-up has a capacity of four 20 MW turbines (4C Offshore n.d.). Blended Design has been used to explore the design space and determine the ship parameters for the direct competitor, the 20MW Moonshot. This Moonshot concept is designed to operate in a market with only 20 MW turbines for only one year. 1,532,160 ship configurations were investigated. Firstly, optimal design ranges were determined with cost for motion compensation levels of €0 to €10,000/(t·m). The actual cost would probably be somewhere in that range. The results are shown in Figure 23.

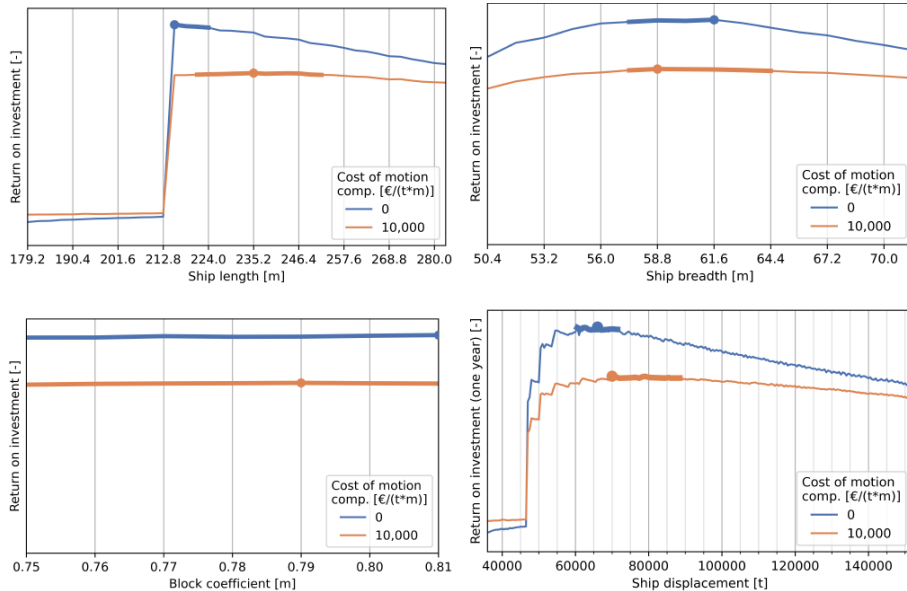


Figure 23: Visualization of the financial performance results for the 20MW Moonshot.

The optimal design ranges reveal an overlap when looking at the two different cost levels. An optimal displacement for both cost levels can be found around 70,000 tonnes. Following a slightly different approach than earlier, the displacement will be fixed at this value to find the optimal ship parameters for best seakeeping performance within this displacement. The results from this analysis are shown in Figure 24. Based on the results from both the financial and seakeeping performance, an optimal configuration can be selected.

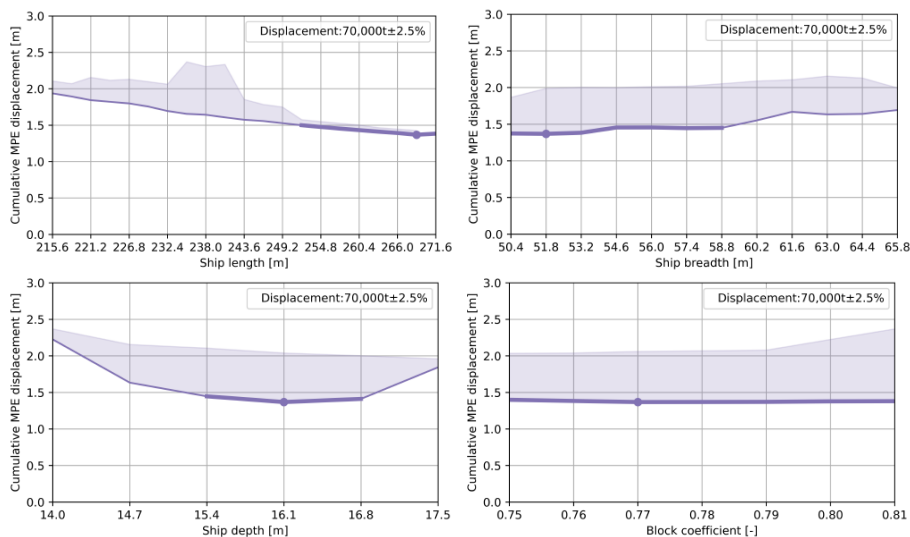


Figure 24: Visualization of the seakeeping performance results for the 20MW Moonshot with a fixed displacement.

After selecting the optimal configuration for the 20MW Moonshot, the day rate, number of installed turbines per year, and the cost per installed MW were extracted from Blended Design. The same metrics were calculated for the NG-20000X jack up, an SSCV, and Huisman's windfarm installation vessel concept. The number of turbines installed per year for those

solutions was determined based on estimated cycle times of the operational cycles. With an assumed day rate, derived from literature or internal knowledge at UDSBV, the cost per installed MW was calculated. These values were then compared to the installation cost per MW of the 20 MW Moonshot.

**Table 9: Comparison of different installation solutions to benchmark Moonshot.**

Parameter	NG-20000X	SSCV	Huisman's WIV concept	20 MW Moonshot
Sailing speed [kn]	11	10	12	13
Cargo capacity (20 MW turbines) [-]	4	-	-	5
Workability [-]	0.6	0.6 <sup>+</sup>	0.6 <sup>+</sup>	0.78
Day rate installation vessel [€/day]	375,000	750,000	750,000	260,000*
Day rate feeder vessels [€/day]	-	2x 50,000	2x 50,000	-
Day rate harbour crane [€/day]	-	32,000	32,000	-
Installed turbines per year [-]	110	165	179	180
<b>Cost per installed MW [€/MW]</b>	<b>50,900</b>	<b>80,100</b>	<b>73,900</b>	<b>21,500*</b>

\* Profit margins are not reflected in the day rates and installation cost per MW of Moonshot, whereas in the others it is included.

<sup>+</sup> Actual workability of the installation vessels is higher. However, it is assumed that the workability is dictated by the offshore transfer from the feeder barges or vessels.

The benchmarking revealed that Moonshot is a more efficient and cost-effective solution, capable of installing a larger number of turbines per year at a considerably lower cost per MW compared to other solutions. The results of the benchmarking show the potential of Moonshot in comparison to other solutions as a competitive and cost-efficient offshore wind turbine installation solution. Above all, since Moonshot is a floating solution and has no interaction with the seabed, it would remain feasible in areas where jack-up vessels might no longer be feasible in the future. Overall, these findings underscore the cost-effectiveness and competitive advantage of the Moonshot concept in the offshore wind industry, positioning it as a promising solution for the evolving demands of the sector.

## CONCLUSIONS

This paper introduced a novel installation solution for offshore wind turbine installation, named Moonshot. The development process involved a combination of UDSBV's Controlled Innovation and Blended Design. With Controlled Innovation functions and design aspects were identified. An evaluation of design aspects revealed the ones that required special attention. These included the choice of lifting equipment, size and mass properties of wind turbine components, and the deck layout. Since Moonshot is a monohull solution that will install turbines while afloat, it would be more susceptible to waves than other existing WTIVs. Therefore, seakeeping assessment is deemed to be important. Modifications to the Blended Design model were made to accommodate Moonshot's unique characteristics and to assess seakeeping performance. With Blended Design, different scenarios were analyzed on both financial and seakeeping performance to explore the design space of Moonshot and elucidate optimal design parameters. The results revealed a disparity when optimizing for financial or seakeeping performance. To balance these factors, a penalty mechanism was introduced, resulting in new optimal ship configurations. Furthermore, Moonshot was benchmarked against other wind turbine solutions, such as jack-ups and SSCVs. Blended Design was used to determine optimal design parameters for a direct competitor. Then, the cost per MW of the other solutions was compared to the optimal 20 MW Moonshot. The comparison showed that Moonshot could be a viable alternative in the offshore wind turbine installation sector.

## CONTRIBUTION STATEMENT

**J.J. de Ridder:** Conceptualization; formal analysis; investigation; methodology; project administration; validation; visualization; writing – original draft. **J.D. Stroot:** Conceptualization; resources; supervision; writing – review and editing. **A.A. Kana:** Conceptualization; supervision; writing – review and editing.

## ACKNOWLEDGEMENTS

This work was performed as part of the MSc thesis for the lead author, (de Ridder 2023). The thesis was performed in Marine Technology at Delft University of Technology and the authors would like to acknowledge both Delft University of Technology and Ulstein Design and Solutions B.V. for their support of this research.

## REFERENCES

- 4C Offshore. (n.d.). *NG-20000X*. Retrieved from <https://www.4c offshore.com/vessels/vessel-ng-20000x-vid2304.html>
- Asgarpour, M. (2016). Chapter 17 - Assembly, transportation, installation and commissioning of offshore wind farms. In C. Ng, & L. Ran, *Offshore Wind Farms - Technologies, Design & Operation* (pp. 527-541). Woodhead Publishing. doi:10.1016/B978-0-08-100779-2.00017-9

- Attari, A., Olayinka Okuyemi, G., Goormachtigh, J., Møller Christensen, J., Tang Kristensen, J., Koch Nielsen, J., . . . Rolland, Y. (2014). *3.1 - WP Framework/Industry Challenges Report – Novel vessels and equipment*. LEANWIND - Logistic Efficiencies And Naval architecture for Wind Installations with Novel Developments.
- Bhattacharya, R. (1973). *Dynamics of Marine Vehicles*. John Wiley & Sons Ltd.
- BVG Associates. (2019). *Guide to an offshore wind farm - Updated and extended*. The Crown Estate and the Offshore Renewable Energy Catapult.
- de Ridder, J. J. (2023). *Beyond Jack-Ups: A Moonshot for Future Offshore Wind Turbine Installation Vessels for an Uncertain Market*. Delft, The Netherlands: Delft University of Technology.
- Det Norske Veritas AS. (2017). *DNV-RP-C205: Recommended practice: Environmental Conditions and Environmental Loads*. Høvik, Norway.
- Díaz , H., & Guedes Soares, C. (2023). Approach for Installation and Logistics of a Floating Offshore Wind Farm. *Journal of Marine Science and Engineering*. doi:10.3390/jmse11010053
- Djupevåg Eri, S. (2015). *Analysis of Operability in Installing Heavy Subsea Modules*. Stavanger, Norway: University of Stavanger.
- EnergyFacts.eu. (2019). *Revolutionary Construction Methodology for Arcadis Ost 1 Offshore Wind Farm*. Retrieved from <https://www.energyfacts.eu/revolutionary-construction-methodology-for-arcadis-ost-1-offshore-wind-farm/>
- Foxwell, D. (2022). *Warning issued that offshore wind won't have enough foundation installation*. Retrieved from Riviera: <https://www.rivieramm.com/news-content-hub/news-content-hub/warning-issued-that-offshore-wind-sector-wont-have-enough-foundation-installation-vessels-71561>
- GustoMSC. (n.d.). *NG-20000X brochure*. Retrieved from <https://www.nov.com/-/media/nov/files/products/rig/marine-and-construction/ng-20000x/ng-20000x-brochure.pdf>
- Heerema Marine Contractors. (2020). *Sleipnir*. Retrieved from <https://www.heerema.com/heerema-marine-contractors/fleet/sleipnir>
- Herman, S. A. (2002). *Offshore Wind Farms - Analysis of Transport and Installation Costs*. TNO.
- Iberdrola. (n.d.). *Wiking Offshore Wind Farm*. Retrieved from <https://www.iberdrola.com/about-us/what-we-do/offshore-wind-energy/wiking-offshore-wind-farm>
- Jensen, J. J., Mansour, A. E., & Olsen, A. S. (2004). Estimation of ship motions using closed-form expressions. *Ocean Engineering*, 61-85. doi:10.1016/S0029-8018(03)00108-2
- Jiang, Z. (2021). Installation of offshore wind turbines: A technical review. *Renewable and Sustainable Energy Reviews*, 1364-0321. doi:10.1016/j.rser.2020.110576.
- Kaiser, M. J., & Snyder, B. (2011). *Offshore Wind Energy Installation and Decommissioning Cost Estimation in the U.S. Outer Continental Shelf*. Herndon, VA: U.S. Dept. of the Interior, Bureau of Ocean Energy Management, Regulation and Enforcement.
- Kuhn, F., Liebach, F., Matthey, T., Schlosser, A., & Zivansky, J. (2023). *How to succeed in the expanding offshore wind market*. McKinsey & Company.
- Matsui, S., Shinomoto, K., Sugimoto, K., & Ashida, S. (2021). Development of Simplified Formula for Froude-Krylov Force of 6-DOFs Acting on Monohull Ship. *Journal of the Japan Society of Naval Architects and Ocean Engineers*, 9-19. doi:10.2534/jjasnaoe.32.9
- Netherlands Wind Energy Association. (2023). *(Dutch) Windmolens op zee niet hoger dan 1000 voet*. Retrieved from <https://www.nwea.nl/windmolens-op-zee-niet-hoger-dan-1000-voet/>
- Nikitas, G., Bhattacharya, S., & Vimalan, N. (2020). Chapter 16 - Wind Energy. In T. Letcher, *Future Energy (third edition)* (pp. 331-355). Elsevier.
- Nørkaer Sørensen, J. (1984). On the Calculation of Trajectories for Blades Detached from Horizontal Axis Wind Turbines. *Wind Engineering*, 160-175. doi:<https://www.jstor.org/stable/43749983>
- NORWEP. (2022). *Global Offshore Wind: Annual Market Report 2022*. OSLO: Renewable Consulting Group .
- Parkinson, S. B., & Kempton, W. (2022). Marshaling ports required to meet US policy targets for offshore power. *Energy Policy*. doi:10.1016/j.enpol.2022.112817
- Quancard, R., Girandier, C., & Robic, H. (2019). *D.4.2 – Design Brief: Specifications of a generic wind turbine*. INNOSEA (INS).
- Richmond, M., Balaam, T., Causon, P., Leimeister, M., Kolios, A., & Brennan, F. (2018). Multi-Criteria Decision Analysis for Benchmarking Human-Free Lifting Solutions in the Offshore Wind Energy Environment. *Energies*. doi:10.3390/en11051175.
- Rijntalder, H. (2023). *Recommended maximum height for offshore windturbines*. Retrieved from Pondera consult: [https://ponderaconsult.com/en/ponderacontent/recommended\\_maximum\\_height\\_for\\_offshore\\_windturbines/#:~:text=A%20workgroup%20on%20the%20issue,the%20developments%20of%20wind%20turbines](https://ponderaconsult.com/en/ponderacontent/recommended_maximum_height_for_offshore_windturbines/#:~:text=A%20workgroup%20on%20the%20issue,the%20developments%20of%20wind%20turbines).
- Riviera Newsletters. (2010). *Interview with Nick Wessels (Ulstein Design & Solutions BV) in Concept quickens installation of offshore turbines*. Retrieved from <https://www.rivieramm.com/news-content-hub/news-content-hub/concept-quickens-installation-of-offshore-turbines-45123>
- Robinson, R., & Futado, I. (2022). Alternatives to Conventional Offshore Fixed Wind Installation. *Offshore Technology Conference*. Houston, TX. doi:10.4043/31986-MS
- Saipem. (n.d.). *Hywind*. Retrieved from <https://www.saipem.com/en/saipem-worldwide-projects/hywind-floating-wind-turbines>

- Schouten, E. (2018). *Monohull versus Semi-submersible for offshore heavy lift crane operations*. Delft, The Netherlands: Delft University of Technology.
- Sen, D. T., & Vinh, T. C. (2016). Determination of Added Mass and Inertia Moment of Marine Ships Moving in 6 Degrees of Freedom. *International Journal of Transportation Engineering and Technology*, 8-14. doi:10.11648/j.ijtet.20160201.12
- Sergiienko, N. Y., da Silva, L. S., Bachynski-Polić, E. E., Cazzolato, B. S., Arjomandi, M., & Ding, B. (2022). Review of scaling laws applied to floating offshore wind turbines. *Renewable and Sustainable Energy Reviews*, 160-175. doi:10.1016/j.rser.2022.112477
- Streatfeild, C., Hoyle, M., Edwards, D., Hodged, B., Osborne, J., Mallett, C., . . . Frampton, M. (2013). *Guidelines for the Selection and Operation of Jack-ups in the Marine Renewable Energy Industry*. London, UK: RenewableUK.
- Ulstein. (2023). *ULSTEIN U-STERN - smart monopile installation on DP*. Retrieved from <https://ulstein.com/news/ulstein-u-stern-smart-monopile-installation-on-dp>
- United Nations. (n.d.). *Causes and Effects of Climate Change*. Retrieved 2023, from <https://www.un.org/en/climatechange/science/causes-effects-climate-change>
- Uraz, E. (2011). *Offshore Wind Turbine Transportation & Installation Analyses. Planning Optimal Marine Operations for Offshore Wind Projects*. Gotland University. Visby, Sweden: Offshore Energy.
- van Bruinessen, T. M. (2016). *Towards controlled innovation of complex projects. A social-technological approach to describing ship design*. Delft, The Netherlands: Delft University of Technology.
- Van Lynden, C., van Winsen, I., Westland, C. N., & Kana, A. A. (2022). Offshore wind installation vessels: Generating insight about the driving factors behind the future design. *International Journal of Maritime Engineering*, 164(A2). doi:10.5750/ijme.v164iA2.1175
- Vis, I. F., & Ursavas, E. (2016). Assessment approaches to logistics for offshore wind energy installation. *Sustainable Energy Technologies and Assessments*, 80-91. doi:10.1016/j.seta.2016.02.001
- WindEurope. (2020). *Offshore wind in Europe*. Retrieved from <https://windeurope.org/wp-content/uploads/files/aboutwind/statistics/WindEurope-Annual-Offshore-Statistics-2019.pdf>
- Zwaginga, J. J. (2020). *Exploring Market Uncertainty in Early Ship Design*. Delft, The Netherlands: Delft University of Technology.
- Zwaginga, J. J., Stroo, J. D., & Kana, A. A. (2021). Exploring market uncertainty in early ship design. *International Journal of Naval Architecture and Ocean Engineering*, 13, 352-366. doi:10.1016/j.ijnaoe.2021.04.003.